

## Mantle geodynamics and source domain of the East Vietnam Sea opening- induced volcanism in Vietnam and neighboring regions

Nguyen Hoang<sup>1,2,\*</sup>, Shinjo Ryuichi<sup>3</sup>, Tran Thi Huong<sup>1</sup>, Le Duc Luong<sup>1,2</sup>, Le Duc Anh<sup>2,4</sup>

<sup>1</sup>*Institute of Geological Sciences, VAST, Vietnam*

<sup>2</sup>*Graduate University of Science and Technology, VAST, Vietnam*

<sup>3</sup>*Department of Physics and Earth Sciences, University of the Ryukyus, Nishihara, Okinawa 903-0213, Japan*

<sup>4</sup>*Institute of Marine Geology and Geophysics, VAST, Vietnam*

\*E-mail: [nghoang@igs.vn.vast.vn](mailto:nghoang@igs.vn.vast.vn)/[hoang\\_geol@hotmail.com](mailto:hoang_geol@hotmail.com)

Received: 2 June 2021; Accepted: 30 September 2021

©2021 Vietnam Academy of Science and Technology (VAST)

### Abstract

The spreading of the East Vietnam Sea (EVS, also known as Bien Dong, or the South China Sea), leading to the occurrence of syn-spreading (33-16 Ma) and post-spreading (< 16 to present) volcanism. Syn-spreading magma making up thick layers of tholeiitic basalt with a geochemical composition close to the refractory and depleted mid-ocean ridge basalt (MORB) is mainly distributed inside the EVS basin. The post-spreading magma is widely distributed inside the basin and extended to South and SE China, Hainan island, Southern Laos (Bolaven), Khorat Plateau (Thailand), and Vietnam, showing the typical intraplate geochemistry. Basaltic samples were collected at many places in Indochina countries, Vietnam's coastal and continental shelf areas, to analyze for eruption age, petrographical, geochemical, and isotopic composition to understand the similarities and differences in the mantle sources between regions. The results reveal that basalts from some areas show geochemical features suggesting they were derived subsequently by spinel peridotite and garnet peridotite melting, forming high-Si, low-Mg, and low-Ti tholeiitic basalt to low-Si, high-Mg, and high-Ti alkaline basalt with the trace element enrichment increasing over time. Other basalts have geochemical and isotopic characteristics unchanged over a long period. The post-spreading basalt's radiogenic Sr-Nd-Hf-Pb isotopic compositions show different regional basalts distribute in the various fields regardless of eruption age, suggesting that their mantle source feature is space-dependent. The post-EVS spreading basalts expose the regional heterogeneity, reflecting the mixture of at least three components, including a depleted mantle (DM) represented by the syn-EVS spreading source, similar to the DUPAL-bearing Indian MORB source; an enriched mantle type 1 (EM1), and type 2 (EM2). The DM may interact and acquire either EM1 or EM2 in the sub-continental lithospheric mantle; as a result, different eruption at different area acquires distinct isotopic signature, reflecting the heterogeneous nature of the subcontinental lithospheric mantle. The study proposes a suitable mantle dynamic model that explains the EVS spreading kinematics and induced volcanism following the India - Eurasian collision from the Eocene based on the research outcomes.

**Keywords:** East Vietnam Sea, syn- and post-spreading basalt, lithospheric mantle, mantle flow.

---

*Citation:* Nguyen Hoang, Shinjo Ryuichi, Tran Thi Huong, Le Duc Luong, Le Duc Anh, 2021. Mantle geodynamics and source domain of the East Vietnam Sea opening- induced volcanism in Vietnam and neighboring regions. *Vietnam Journal of Marine Science and Technology*, 21(4), 393–417.

## INTRODUCTION

In the Cenozoic period, the East Vietnam Sea (EVS) opening process followed the continental breakup that led to the oceanic crust extension. The Red river faulting activity began 35 to about 15 million years ago, extruding the lithosphere a distance of several hundred kilometers (700 km?) [1–3]. Taylor and Hayes (1983) [4], followed by Briais et al., (1993) [5], argued that the entire EVS was formed by oceanic-like crustal extension between 32 and 16 million years ago (Oligocene - Miocene). Barckhausen et al., (2014) [6], however, suggested that the EVS opening ended 20.5 million years ago, about 4 million years earlier, due to the faster rate of later oceanic crust extension. Researchers of the EVS tectonics, such as Rangin et al., (1995) [7] and Clift et al., (2008) [7], argue that the Red river shearing activity is difficult to cause a significant spreading of the EVS. Other researchers (e.g., [4, 9]) argued that extension tectonics in East and Southeast Asia occurred in the Mesozoic related to the proto-Pacific plate subduction before the India-Eurasian collision.

Many EVS-opening tectonic models have been introduced over the years. But none is satisfied that the spreading occurred once or for many times [5, 9–12]. Besides, are the Northwest and East sub-basin opened before or simultaneously with the Southwestern sub-basin? [5, 10, 13].

The EVS opening tectonics led to magma activities inside the basin and widely spread on Southern mainland China, Hainan island, Indochina, and Thailand, especially in the post-EVS spreading period (< 16 Ma). Basalt samples were collected in Vietnam, Southern Laos, and Southeast Thailand to analyze major and trace elements, Sr-Nd-Pb isotopic ratios, and radiometric age data. The data are combined and compared with nearby basalt regions (such as Hainan island) to determine the similarity and difference in their mantle source, melting mechanism, and forming conditions. The report proposes an appropriate geodynamic model explaining the relationship between the EVS opening and volcanism following the Indian and Eurasian continent collision tectonics since the Eocene era.

## EAST VIETNAM SEA OPENING PERIODS

Summarizing the result of magnetic anomalies and stratigraphic drilling data collected over the EVS survey periods, especially the IODP 349 expedition [20, 21], many researchers have drawn several conclusions as follows. The opening of EVS began in the northeast about 33 million years ago (Ma). About 23.6 Ma, the Eastern sub-basin spreading axis jumped about 20 km to the south. This time coincided with the ignition of the extension in the southwestern sub-basin, with a spreading axis running southwest about 400 km from 23.6 Ma to 21.5 Ma [20, 21]. The Eastern sub-basin extension ceased about 15 Ma, and in the Southwestern sub-basin, about 16 Ma [20]. The initiation and cessation of oceanic crust spreading periods obtained in the IODP 349 survey coincide with the ES opening model by Taylor and Hayes (1983) [4] and Briais et al., (1993) [5] rather than other tectonic models [20] (fig. 1). This opening mode is essentially similar to the Japan Sea's spreading, where the initial extension center formed in the northeast ignited by a left-lateral strike-slip motion [22]. The spreading axis gradually migrated west-southwest to the south-southwest, where the spreading stopped about 15 Ma [22–24]. In contrast to the EVS opening, the whole Japan Sea opening process occurred approximately 21 Ma to 15 Ma [25].

In summary, although the mechanism of the rifting that forms the ES is different, for example, the plate subduction and stretching of Taylor and Hayes (1982) [4] compare with the theory of the lithospheric escape along the Red river shear zone of Tapponnier et al., (1982, 1986) [2, 3] and Briais et al., (1993) [5] are convincing enough or not. However, the age of the EVS opening provided by the models is relatively similar [20, 21].

The International Ocean Discovery Program (IODP) expeditions 349 and 367/368 in the East Vietnam Sea in early 2014 and 2017 obtained many actual results to understand the geology and opening tectonics of the EVS [20, 21, 26, 27]. For the first time, deep-sea drilling was carried out in different areas along the ES spreading axis to study sediments, volcanic products, and geological structures to identify

tectonic processes, mechanisms, dynamics, and extending periods leading to the formation of the EVS [20, 21, 26, 27].

### THE EVS OPENING TECTONICS AND MAGMA ACTIVITY

Lithospheric extension and magma activity are in a physical relationship. Depending on the type of extension (pure shear vs. simple shear), the extension coefficient ( $\beta$ ), which is the ratio of the lithosphere thickness before and after the extension [28], whether magma can occur. The resulting magma's intensity depends on the

lithosphere extension rate; for example, more magma occurs in the mid-ocean ridges with the rapid spreading rate as the Pacific Ocean [29], compared to the Indian Ocean [30–32].

### Syn- EVS spreading magmatism

As mentioned above, the East Vietnam Sea opening process occurred between 33 million years and (about) 15.5–16 million years. The magma that happened in this period is called syn-spreading. Some small amount of syn-spreading magma is distributed in the northern margin but mainly inside the ES basin.

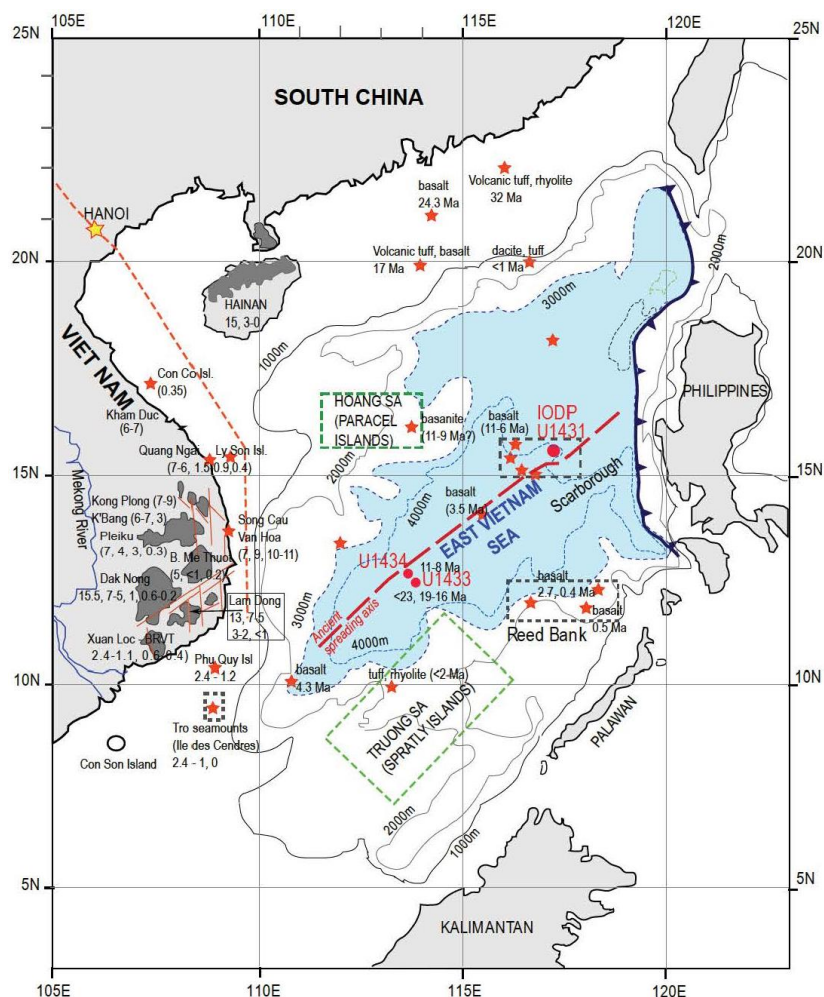


Figure 1. Distribution map of dispersed basalt regions following the East Vietnam Sea spreading in Vietnam and neighboring areas. The number next to the places is the eruption age (in million years) of KC09.31/16–20 national project (unpublished), others from [7, 14]). Of places in the EVS basin are after [4, 12, 15–19]. The ancient EVS spreading axis and deep ODP drill sites are after [20, 21]

The IODP 349 expedition had conducted four deep-sea drillings at 4 locations in the spreading axis area, but only at one site in the Eastern sub-basin (U1431), and two in the southwestern sub-basin (U1433) have discovered volcanic rocks. At borehole U1431E (15°22.538'N, 116°59.9903'E) at 118 meters below a depth of 890 m from the sea bottom, 46.7 meters of basalt made by 13 eruptions, divided into two volcanic groups, separated by a layer of hemipelagic sediment of about 3.7 m thick. Both layers of volcanic rock have a massive structure (fig. 1). The volcanic rock is covered by a 282 m thick volcanic-sedimentary layer containing many volcanic rock fragments in phenocrysts such as plagioclase and pyroxene olivine, suggesting volcanic seamounts occurred in the area. According to the description, basalt at borehole U1431E is aphyric, small-grained, and some phyric coarse-grained basalt distributed in massive basalt layers with a phenocryst mineral assemblage containing plagioclase, clinopyroxene ± olivine. On the correlation diagram between SiO<sub>2</sub> and total alkalinity (TAS), the basalt at borehole U1431E is distributed in the mid-ocean ridge basalt (MORB) of the Pacific (or the Indian Ocean) type, different from intraplate basalt (e.g., Hainan island) [21]. At the borehole U1433B (12°55.1313'N, 115°2.8484'E) next to the southwestern sub-basin spreading axis, a basalt layer comprises 45 eruption units with a total thickness of 60.8 m. The basalt layer is divided into two episodes; the upper is 37.5 m thick consisting of pillow lava, followed by the 23.3 m thick layer of massive basalt. Hemipelagic sediments overlie this whole basalt layer. Like basalt collected at borehole U1431E, the borehole U1433B is distributed in the mid-ocean ridge basalt field (MORB) [20, 21].

### Post-EVS spreading magmatism

Magma happened during the 15–16 million years period, is called post-spreading. Post-spreading basalt eruption occurs not only in the EVS basin but widely on the continent in Indochina, Thailand, South and Southeast China [12, 16, 20, 21, 33–36]. Vietnam and Hainan Island are two massive, post-spreading volcanic regions [15, 17, 18, 37–40] (fig. 1). They all have an eruption age from about 15 Ma to

Pliocene - Quaternary (4-0 Ma). As in Vietnam, Hainan island basalt evolved from high SiO<sub>2</sub>, MgO, FeO magma, and low total alkalinity to low SiO<sub>2</sub>, high MgO, and total alkalinity reflecting changes in mantle source composition and increasing melting pressure over time [17, 18, 39–41].

In the deep EVS basin, post-opening eruptions are common around the spreading axis extending from the Northeast sub-basin to the Central and the Southwest sub-basin [20, 21] from about 14 Ma till the present day. Qian et al., (2020) [36] collected a series of volcanic glass and phenocryst samples such as feldspar and biotite in volcanic breccia products in the U1431 core from the East sub-basin [20] belonging to two eruption periods of 11-8 Ma (million years ago) and < 8 Ma to analyze for geochemical and Sr-Nd-Pb isotopic compositions [36]. The aim is to understand geochemical and isotope evolution between eruption phases. The results showed that the volcanic glass and feldspar of two age groups belong to two different geochemical groups. The older one has a relatively depleted isotopic and geochemical composition, fluctuating in a narrow range; the younger group is more enriched Sr and Pb isotopes that vary over a wide range.

Like the post-spreading continental basalt's geochemical evolution, the post-spreading basalt in the EVS basin reveals the evolutionary trend from basalt tholeiite to alkaline and sub-alkaline basalt [15, 16, 18, 20, 21]. This geochemical trend reflects the melting of at least two mantle sources or the melting at increasing melting pressures over time.

### Basalt sampling and analytical procedures

#### Sampling

Basalt samples are collected in the framework of the national project KC.09.31/16–20 on a large scale in Vietnam's continental, coastal, and continental shelf areas and the southwestern deep-sea basin of EVS (Figs. 1, 2a–2f). For reference, samples were also collected on the Bolaven Plateau (Southern Laos) and the Khorat Plateau (Southeastern Thailand). Hon Tro submarine volcanic samples were acquired through international collaboration projects with Petropavlovsk-Kamchatka and Vladivostok, Russia.



*Figure 2.* Outcrops of 7.5 Ma massive tholeiitic layers up to 3 m thick about 8 km southwest of Dak Mil (a); Layers of 0.6-0.4 Ma massive, olivine-bearing sub-alkaline basalt outcropped at Dray Sap waterfall (Krông Nô, Dak Nong) (b); NW wall of Thoi Loi cinder cone at Ly Son island, a blow-up showing representative stratigraphy of a  $2 \times 1$  m section containing parallel layers of volcanic ash, tuff, and lava fragments (bombs) (c); Outcrop of rare 0.9-0.4 Ma massive lava flows at Small Island (Bo Bai, Ly Son); Four visible lava layers with thicknesses varying from 1.2 m to 2 mm separated by brick-red volcanoclastic products (d); 2.4 Ma Hon Tranh volcano ( $1.5 \times 0.5$  km) about 1.5 km south of Phu Quy island (e); Outcrops of 1.2 Ma to 1 Ma massive blocks of sub-alkaline and alkaline-borne mantle xenoliths at Ghenh Hang, Phu Quy island (f)

Samples were processed to study petrography (figs. 3a–3d, Appendix A) and age dating by the K-Ar radiometric method at the Institute for Nuclear Research, Hungarian Academy of Sciences (Debrecen, Hungary), whose procedure is described in detail in [42]. K-Ar age dating was also performed at the Far East Geological Institute, Far East Branch, RAS, Vladivostok, following the procedure given in Ignat'ev et al., (2010) [43]. Some of

the K-Ar age samples were reanalyzed using Ar-Ar and zircon U-Pb age dating [44] to verify the accuracy of the K-Ar analysis. The accuracy of the K-Ar method is  $(1\sigma) \pm 0.1$ – $0.2$  for ages  $< 1$  Ma, and about  $(1\sigma) \pm 0.3$ – $0.4$  for ages  $> 5$ – $7.5$  Ma. The geochemical composition was acquired using XRF and ICP-MS, and radiogenic isotopes such as Sr, Nd, Hf, and Pb were analyzed using an MC-ICP-MS.

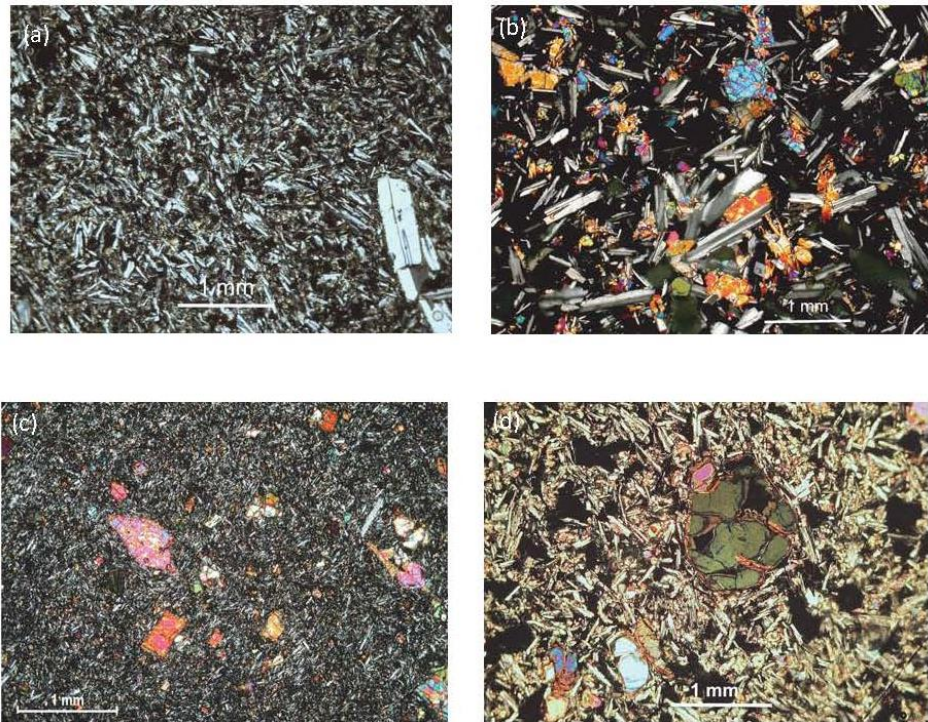


Figure 3. Photomicrographs of 7.5 Ma apyric tholeiite from Dak Mil showing a rare plagioclase phenocryst among mostly needle-shaped plagioclase microlitic groundmass: plane polarized light (a); A thin section of 0.6-0.4 Ma intersertal-textured sub-alkaline basalt from Dray Sap waterfall, showing phenocrysts of olivine and plagioclase on the plagioclase and clinopyroxene microlitic and volcanic glass groundmass: cross polarized light (b); Photomicrographs of 1 Ma phyric sub-alkaline basalt from Ly Son island, showing euhedral or subhedral olivine in the phenocryst on the microlitic plagioclase, Fe-Ti oxide, and volcanic glass groundmass: cross polarized light (c); A ca. 1 Ma alkaline phyric-textured with olivine phenocryst in the microlitic plagioclase and volcanic glass groundmass from Phu Quy island: cross polarized light (d)

The analysis was carried out at the Department of Physics and Earth Sciences, Ryukyu University, Nishihara (Okinawa, Japan), the Center of Mineralogy and Petrology, Graz University, Austria, and at the Geological

Survey of Japan, Tsukuba, Ibaraki. Analytical procedures, accuracy, and reliability of each method are detailed in [45, 46]. Age, geochemical and isotopic compositions of the representative basalts are presented in table 1.

Table 1. Age, geochemical and Sr-Nd-Pb isotopic compositions of post-East Vietnam Sea spreading in Vietnam and its vicinity

Sample ID	BLA-6	Ly Son 2	Kham Duc 1	G Yen-1c	G Da Dia-2	K'Bang
No.	1	2	3	4	5	6
Age (Ma)	7, 1	1.2, 1, 0.4	7-6	6-5	9-7	7-6
SiO <sub>2</sub>	45.22	51.77	52.04	52.72	48.83	50.41
TiO <sub>2</sub>	2.17	1.6	1.76	1.45	2.39	1.55
Al <sub>2</sub> O <sub>3</sub>	14.52	14.99	14.23	14.52	15.68	15.11
Fe <sub>2</sub> O <sub>3</sub> T	11.04	10.22	10.69	9.70	11.42	10.13
MnO	0.15	0.14	0.14	0.14	0.16	0.16
MgO	11.58	6.95	7.26	6.80	6.32	5.43

CaO	9.02	7.64	8.69	8.91	7.77	9.30
Na <sub>2</sub> O	2.44	3.2	3.17	2.73	3.36	3.03
K <sub>2</sub> O	1.82	1.21	1.15	0.54	1.66	1.21
P <sub>2</sub> O <sub>5</sub>	0.33	0.36	0.28	0.20	0.59	0.31
La	35.62	19.7	13.91	16.86	32.01	18.47
Ce	70.97	39.18	28.70	35.91	64.30	36.50
Pr	8.01	4.5	3.67	4.74	7.70	4.45
Nd	32.78	19.94	16.01	21.07	31.32	18.36
Sm	6.52	4.78	4.22	5.76	6.85	4.31
Eu	2.03	1.6	1.47	2.16	2.20	1.55
Gd	6.16	4.95	4.57	6.29	7.04	4.61
Tb	0.87	0.72	0.71	0.97	1.01	0.69
Dy	4.36	3.89	4.01	5.64	5.71	3.88
Ho	0.79	0.73	0.76	1.03	1.07	0.74
Er	2.1	1.93	1.93	2.63	2.79	1.90
Tm	0.26	0.25	0.26	0.34	0.39	0.25
Yb	1.63	1.51	1.55	2.03	2.32	1.56
Lu	0.22	0.21	0.21	0.28	0.33	0.22
<sup>87</sup> Sr/ <sup>86</sup> Sr	0.704288	0.705673	0.704491	0.703969	0.704564	0.704201
<sup>143</sup> Nd/ <sup>144</sup> Nd	0.512834	0.512584	0.512816	0.512835	0.512839	0.512792
$\epsilon_{Nd}$	3.83	-0.96	3.47	3.84	3.93	3.01
<sup>206</sup> Pb/ <sup>204</sup> Pb	18.587	18.307	19.028	18.571	18.869	18.531
<sup>207</sup> Pb/ <sup>204</sup> Pb	15.626	15.628	15.713	15.715	15.693	15.649
<sup>208</sup> Pb/ <sup>204</sup> Pb	39.929	38.413	39.209	38.989	39.206	38.988
D7/4Pb	12	15.3	15.9	21.1	15.7	14.9
D8/4Pb	83.0	66.5	57.7	90.8	76.6	95.7
Sample ID	<i>B Thuan</i>	<i>Van Hoa</i>	<i>Dak Mil</i>	<i>Soc Lu</i>	<i>Dat Do</i>	<i>Hon Tro</i>
No.	7	8	9	10	11	12
Age (Ma)	7-5.5	11-8	15.4, 7, 0.9-0.2	4.5, 0.32	0.7-0.6	2.4, 1.1, 0
SiO <sub>2</sub>	53.2	48.30	50.53	55.82	44.24	48.51
TiO <sub>2</sub>	1.64	2.19	1.7	1.53	2.27	2.38
Al <sub>2</sub> O <sub>3</sub>	15.11	15.13	14.51	15.75	12.68	14.84
Fe <sub>2</sub> O <sub>3</sub> T	10.09	10.95	11.1	8.79	11.6	11.32
MnO	0.14	0.16	0.15	0.12	0.18	0.16
MgO	6.4	6.52	6.97	4.20	10.28	6.56
CaO	8.57	7.39	8.54	6.39	9.86	7.27
Na <sub>2</sub> O	3.48	3.12	2.78	4.22	3.95	4.49
K <sub>2</sub> O	0.8	1.59	0.41	2.34	2.04	3.08
P <sub>2</sub> O <sub>5</sub>	0.17	0.59	0.18	0.42	0.91	0.84
La	15.34	31.17	10.96	43.9	84.79	61.85
Ce	25.93	63.31	23.57	79.1	162.60	118.14
Pr	3.33	7.65	3.25	8.88	19.41	12.36
Nd	16.37	30.91	17.10	33.7	82.46	48.15
Sm	4.39	6.67	4.74	7.6	15.57	8.87
Eu	1.65	2.18	1.60	2.39	4.18	2.71
Gd	6.08	6.99	5.77	7	13.98	8.3
Tb	0.90	1.02	0.81	1	1.50	1.17
Dy	5.76	5.65	5.29	5.3	8.77	5.9
Ho	0.98	1.08	0.88	0.9	1.31	1.09
Er	2.89	2.83	2.73	2.3	3.87	2.88

Tm	0.36	0.39	0.32	0.28	0.45	0.36
Yb	2.14	2.37	2.11	1.6	2.75	2.19
Lu	0.29	0.34	0.26	0.22	0.31	0.32
<sup>87</sup> Sr/ <sup>86</sup> Sr	0.704229	0.704995	0.703810	0.704803	0.704228	0.704744
<sup>143</sup> Nd/ <sup>144</sup> Nd	0.512955	0.512863	0.512888	0.512734	0.512800	0.512704
$\epsilon_{Nd}$	6.18	4.38	4.87	1.87	3.16	1.29
<sup>206</sup> Pb/ <sup>204</sup> Pb	18.558	18.620	18.545	18.200	18.056	18.312
<sup>207</sup> Pb/ <sup>204</sup> Pb	15.588	15.610	15.575	15.560	15.520	15.621
<sup>208</sup> Pb/ <sup>204</sup> Pb	38.596	38.649	38.626	38.365	38.335	38.760
D7/4Pb	8.6	10.0	7.3	9.7	7.2	14.5
D8/4Pb	53.2	51.0	58.8	73.2	87.8	99.3
<i>Sample ID</i>	<i>Phu Quy</i>	<i>Cua Tung</i>	<i>Bolaven 1</i>	<i>Bolaven 2</i>	<i>Bolaven 3</i>	<i>Khorat</i>
<i>No.</i>	<i>13</i>	<i>14</i>	<i>15</i>	<i>16</i>	<i>17</i>	<i>18</i>
Age (Ma)	2.4, 1.2	< 1	8	3	< 1.2	< 3 - 1
SiO <sub>2</sub>	49.14	48.49	51.82	48.34	43.81	46.89
TiO <sub>2</sub>	2.34	2.17	1.86	1.81	2.52	1.92
Al <sub>2</sub> O <sub>3</sub>	14.08	14.29	14.64	14.29	14.55	14.37
Fe <sub>2</sub> O <sub>3</sub> T	11.31	10.50	11.28	12.63	13.32	11.58
MnO	0.15	0.130	0.16	0.16	0.17	0.16
MgO	8.57	7.36	6.27	7.73	8.34	7.85
CaO	8.88	7.44	8.49	7.74	8.06	9.44
Na <sub>2</sub> O	2.9	3.12	3.08	3.40	4.30	2.38
K <sub>2</sub> O	1.98	1.23	0.96	1.61	2.51	1.60
P <sub>2</sub> O <sub>5</sub>	0.49	0.318	0.33	0.51	0.98	0.49
La	35.61	9.30	17.82	33.65	57.67	22.07
Ce	66.99	18.44	34.02	62.18	102.04	50.54
Pr	7.55	2.32	4.42	7.33	12.06	7.19
Nd	32.17	9.92	18.92	29.37	47.49	33.56
Sm	7.37	2.48	4.68	6.57	9.27	8.28
Eu	2.31	0.85	1.56	2.09	2.84	2.69
Gd	7.22	2.45	4.66	6.07	8.06	7.38
Tb	1.06	0.33	0.77	0.91	1.11	0.90
Dy	5.53	1.91	4.42	4.70	5.31	4.63
Ho	1.02	0.34	0.81	0.84	0.90	0.75
Er	2.63	0.88	1.98	1.94	2.00	1.76
Tm	0.32	0.10	0.26	0.24	0.23	0.18
Yb	1.89	0.66	1.67	1.53	1.41	1.13
Lu	0.26	0.10	0.22	0.20	0.17	0.16
<sup>87</sup> Sr/ <sup>86</sup> Sr	0.705008	0.704665	0.704101	0.703902	0.703925	0.703871
<sup>143</sup> Nd/ <sup>144</sup> Nd	0.512711	0.512736	0.512834	0.512846	0.512846	0.512974
$\epsilon_{Nd}$	2.05	1.91	4.02	4.06	4.0	6.55
<sup>206</sup> Pb/ <sup>204</sup> Pb	18.110	18.768	18.690	18.712	18.405	18.237
<sup>207</sup> Pb/ <sup>204</sup> Pb	15.533	15.695	15.641	15.610	15.585	15.545
<sup>208</sup> Pb/ <sup>204</sup> Pb	38.300	39.107	38.835	38.945	38.656	38.245
D7/4Pb	7.8	16.9	12.5	9.1	77.6	7.7
D8/4Pb	75.86	78.94	60.7	68.8	77.62	57.10

Notes: 1) Ba Lang An (n = 8); 2) Ly Son (n = 25); 3) Kham Duc (n = 12); 4) Ghenh Yen (n = 12); 5) Ghenh Da Dia (n = 10); 6) K'Bang (n = 8); 7) Binh Thuan (n = 12); 8) Van Hoa (n = 2); 9) Dac Mil (n = 45); 10) Soc Lu (n = 14); 11) Dat Do (n = 6); 12) Hon Tro (n = 8); 13) Phu Quy (n = 42); 14) Cua Tung (n = 5); 15) Bolaven tholeiite (n = 12); 16) Subalkaline (n = 12); 17) Alkaline (n = 16); 18) Khorat, Thailand (n = 12).

### Analytical results

The geochemical and isotopic data of Vietnam, Thailand, and Bolaven in this study are processed together with data of syn-EVS spreading basalt [20, 21, 47], Hainan island basalt [15–17, 39, 40], Bolaven [48], Khorat [49, this study], and other Vietnam basalt [38, 46, 50, 51]. The Pacific -MORB [29]), and SW- and SE- Indian MORB [31, 52] were shown for comparison.

### Major element compositions

The syn-EVS spreading basalt has  $\text{SiO}_2$  content ranging from 44 wt.% to 53 wt.%, the total alkali content ( $\text{Na}_2\text{O} + \text{K}_2\text{O}$ ) is low, from about 2.5 wt.% to 3.5 wt.% (fig. 4). Most Dak Nong basalt (aged 15.4 Ma to 0.89-0.2 Ma) and the Bolaven tholeiitic samples (15-8 Ma) have the same low total alkalinity ( $\text{Na}_2\text{O} + \text{K}_2\text{O} = 3\text{--}3.5$  wt.%), distributed in the syn-EVS spreading basalt field. Basalts, aged from 6 Ma to 11 Ma such as Ghenh Yen (Binh Son, Quang Ngai), Van Hoa - Cung Son (Phu Yen), Kham Duc (Quang Nam) - K'Bang (Gia Lai) - Vinh Son (Binh Dinh), are mainly tholeiitic or olivine-bearing sub-alkaline basalt, has  $\text{SiO}_2$  in the range of 47–53 wt.%, and total alkalinity approximately 4–6 wt.%, also plot to the

tholeiitic field. Group of 9 Ma basalt including Song Cau - Ghenh Da Dia (Phu Yen) and a few Van Hoa - Cung So samples had higher total alkalinity (from 5 wt.% to 7.5 wt.%) plot to an alkaline field along with the coastal and the continental shelf basalts such as Ly Son, Phu Quy and Hon Tro (IDC) (fig. 4). Another group of basalts having very low  $\text{SiO}_2$  (42–47 wt.%) corresponding to the total alkalinity from 3.5 wt.% to 7 wt.% plot to the basanite/nephelinite field. This group includes Ba Lang An - Sa Ky (7-1 Ma), Trinh Nu - Upper Quang Phu (< 1 Ma), Thong Nhat - Soc Lu (Dong Nai) (4-0.32 Ma) samples, and also 1.2 Ma Bolaven nephelinite and a few post-spreading basanite samples from EVS basin (Yan et al., 2008). Hainan island basalt aged 15, 11-9, 3-0.1 Ma [15–17, 39, 40], having  $\text{SiO}_2$  from 48 wt.% to 53 wt.% and the total alkalinity from 2.5 wt.% to 5.8 wt.%, overlaps partly the Dak Nong tholeiitic and extends into the alkaline field, covering partially Ly Son, Phu Quy, and low- and high-alkaline Bolaven basalts (fig. 4). In summary, the major element composition of post-EVS spreading basalt from Vietnam and neighboring areas reveals an apparent geochemical heterogeneity in space and time.

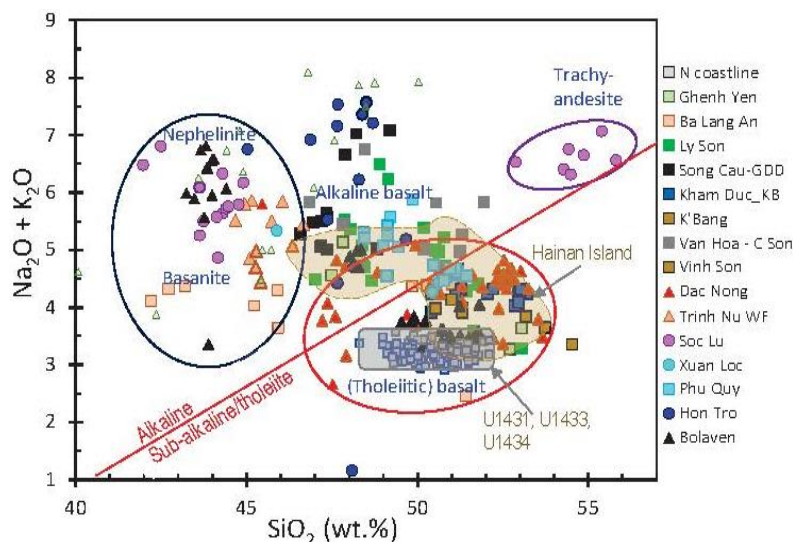


Figure 4.  $\text{Na}_2\text{O} + \text{K}_2\text{O}$  vs.  $\text{SiO}_2$  (TAS) classification diagram for the Vietnam post-EVS spreading basalts. Shown are fields of Dak Nong 15.5-to-0.2 Ma (red contour) and Hainan island 15 (?) - 0 Ma (brown, filled, after [39]). These two fields are nearly overlapped, embedding syn-EVS basalts (U1431, 1433, 1434 after [47]). Also plotted for reference are basalts of post-EVS spreading basalts from the EVS basin (cyan-filled triangles; after [16, 17]). See explanation in the text

Correlation between  $\text{CaO}/\text{Al}_2\text{O}_3$  and  $\text{TiO}_2$  may reflect mineral fractional crystallization and mantle source heterogeneity (fig. 5).  $\text{CaO}/\text{Al}_2\text{O}_3$  is affected slightly by plagioclase and clinopyroxene, is unaffected by olivine fractionation. Most of the Dak Nong tholeiitic basalts plot along with most of the 11-6 Ma tholeiites and ca. 1 Ma coastal basalts, forming a field relatively high  $\text{TiO}_2$  (ca. 1.5–1.7 wt.%) and  $\text{CaO}/\text{Al}_2\text{O}_3$  (0.4–0.65) that is embedded in the field of experimental-defined peridotite melt fractions (A). Many Ly Son, Hon Tro - Phu Quy, and Thong Nhat basalts

create a high- $\text{TiO}_2$  - moderate  $\text{CaO}/\text{Al}_2\text{O}_3$  field (B). Plotting in the B field includes Bolaven nephelinite, Khorat hawaiiite (light-green filled circles, after [49]), and post-spreading basanite from the EVS basin (cyan filled triangles, after [17]). Interestingly, the Hainan basalts, having a wide range of  $\text{TiO}_2$  from about 1.5 wt.% to 3.25 wt.%, spread from field A to B separated from most other regional basalts (fig. 5). The syn-EVS spreading basalts, having the lowest  $\text{TiO}_2$  but moderate to high  $\text{CaO}/\text{Al}_2\text{O}_3$ , plot separately to the left corner in figure 5.

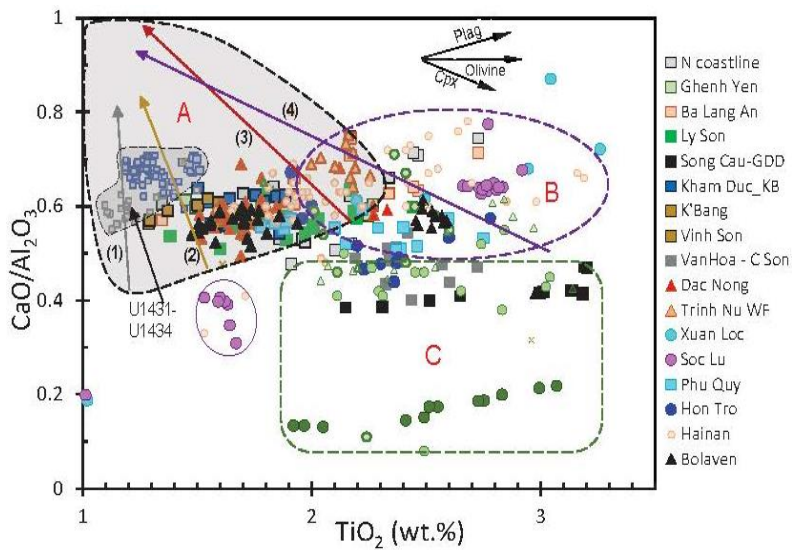


Figure 5. Correlation between  $\text{CaO}/\text{Al}_2\text{O}_3$  and  $\text{TiO}_2$  (wt.%) for Vietnam's post-spreading basalts.

Also plotted for reference are Thailand basalt: light-green filled circles (after [49]), dark-green filled circles (Hoang N, unpublished data); Bolaven basalt are from [48]. Other data sources (syn- and post-EVS basalts, Hainan island) are as of figure 4. Shown is field of experimental peridotite melt fractions (gray-filled contour) of refractory (KBL-1, line 1), relatively fertile (HK-66, line 2), and fertile garnet peridotite (PHN 1611, line 3); and a hybrid peridotite - mafic (pyroxenite, line 4).

Arrows indicate progressive partial melting from low- to high- fraction, and low- to high temperature; after [53–55]. Directions of olivine, clinopyroxene (Cpx) and plagioclase (plagioclase) fractionation. See explanation in the text

#### Trace element compositions

The chondrite normalized rare earth element distribution configuration [56] of post-spreading basalt representing the regions of Vietnam, Laos, Thailand, and Hainan is shown in figure 6. The similarities and differences between the regional basalts are as follows:

Three types of Vietnam basalt (alkaline, sub-alkaline, and tholeiite) have distinct

geochemical enrichment and depletion. The light rare earth (LREE) content of alkaline basalt is 200–250 times higher than the chondrite, while the heavy rare earth (HREE) is only about ten times higher. The difference between tholeiite and sub-alkaline basalt from the chondrite is 50–80 times, 100–120 times, respectively. Note that basalt types converge smoothly at the HREE elements (fig. 6a).

Bolaven basalt types have a rare earth element distribution curve similar to Vietnam basalt, including the enrichment level. The only difference is that the tholeiite has a gentler slope from LREE to HREE, crossing the curve of HREE at thulium (Tm) to ytterbium (Yb) (fig. 6b).

Some alkaline basalt from Hainan island (after [39]) is 150 to 500 times higher than the chondrite. Hainan basalt has a steep slope from LREE to HREE than Vietnam and Bolaven basalt, in which the basalt types intersect at the

HREE elements, from holmium (Ho) to ytterbium (Yb), except those having LREE content higher 500 times compared with the chondrite (fig. 6c).

Alkaline basalt from Khorat (Thailand, this study) has a relatively low rare earth element enrichment, about 150 times higher than the chondrite; however, they have a rather steep slope from LREE to HREE. Khorat hawaiiite (high total alkali basalt) has a low LREE value and a gentle slope to HREE, cutting the alkaline basalt distribution curve at erbium (Er) (fig. 6d).

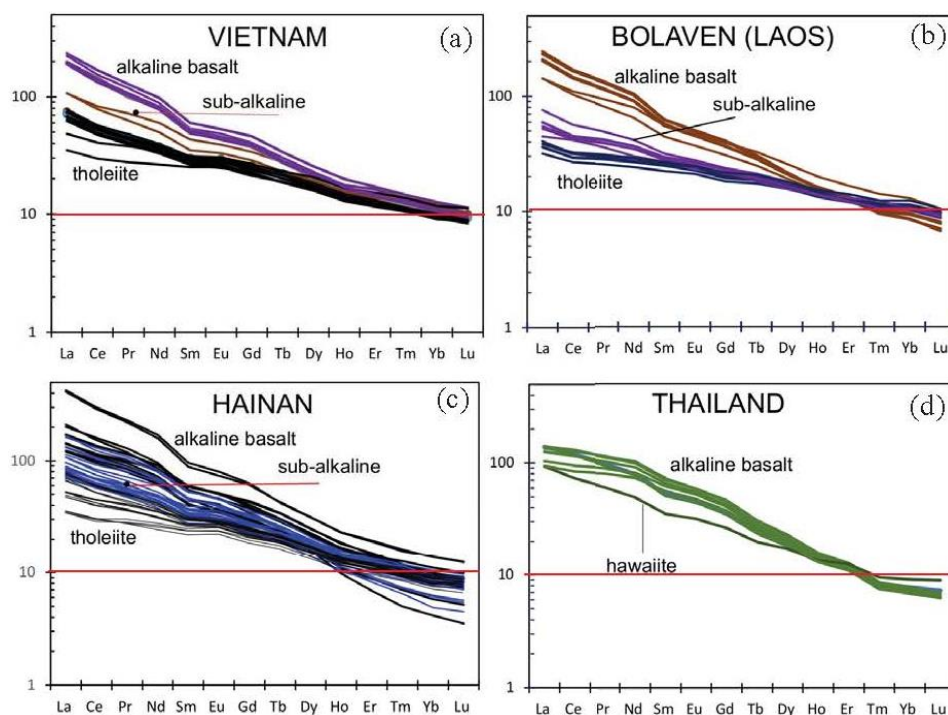


Figure 6. Chondrite rare earth normalized Vietnam, Hainan (after [39]), Bolaven [48] and Thailand (this study) post-spreading basalts. Normalizing data are after [56].

See explanation in the text

#### *Sr-Nd-Pb isotopic compositions*

The regional basalts distribute between the depleted mantle (P-MORB, Southwest and Southeast Indian MORB, after White et al., (1987); Holm (2002) and Mahoney et al., (2002)) and the enriched mantle (EM1 and EM2) [57]. Dak Nong tholeiites and most old 11-6 Ma, Hainan island basalts and a group of Khorat hawaiiite (Thailand 1) plot in a low- $^{87}\text{Sr}/^{86}\text{Sr}$  and high- $^{143}\text{Nd}/^{144}\text{Nd}$  field, intermediately after the isotopic area of syn-EVS

spreading basalt. Ly Son basalt (< 1.2–0.4 Ma) is the most enriched, followed by Phu Quy and Hon Tro (Ile des Cendres), basalt from the SW basin, along the northern coastal area; all form a field limited by  $^{87}\text{Sr}/^{86}\text{Sr}$  at 0.7046–0.7065 and  $^{143}\text{Nd}/^{144}\text{Nd}$  at 0.5128–0.5125. Connecting the depleted and enriched fields are Xuan Loc - Dat Do and several Song Cau - Ghenh Da Dia and Van Hoa - Cung Son samples (fig. 7). Another set of Khorat basalt (Thailand 2) shows equally enriched to the Vietnam continental shelf basalt.

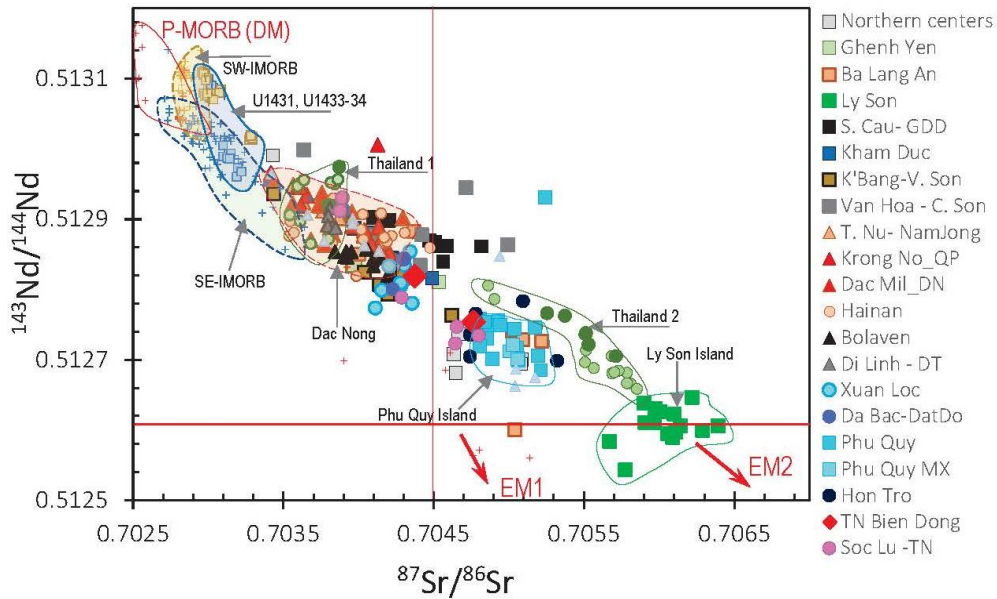


Figure 7. Correlation between  $^{87}\text{Sr}/^{86}\text{Sr}$  and  $^{143}\text{Nd}/^{144}\text{Nd}$  for Vietnam post-spreading basalts. Plotted for reference are syn-EVS spreading basalts [47], Hainan island [15]; Bolaven (Southern Laos) and Khorat (SE Thailand) [48, 49, this study]. Data field of Pacific MORB [29], SW-IMORB [52], SE-IMORB [31, 32]. Fields of the depleted mantle (DM), enriched mantle types 1 and 2 (EM1, EM2) are after [57]

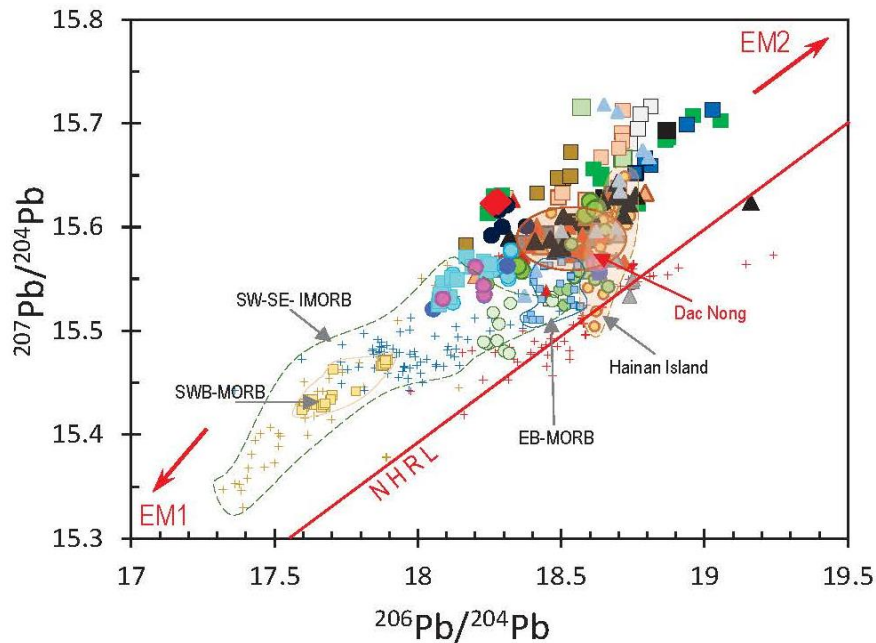


Figure 8a. Correlation between  $^{206}\text{Pb}/^{204}\text{Pb}$  and  $^{207}\text{Pb}/^{204}\text{Pb}$  for post-spreading basalts from Vietnam and its vicinity. Phu Quy island basalts and other from Southeastern region have low  $^{206}\text{Pb}/^{204}\text{Pb}$  values, plotting inside the Indian MORB field. Syn-spreading basalts from East sub-basin (EB-MORB) have higher  $^{206}\text{Pb}/^{204}\text{Pb}$  compared to SW sub-basin (SWB-MORB). Data sources are as in figure 7

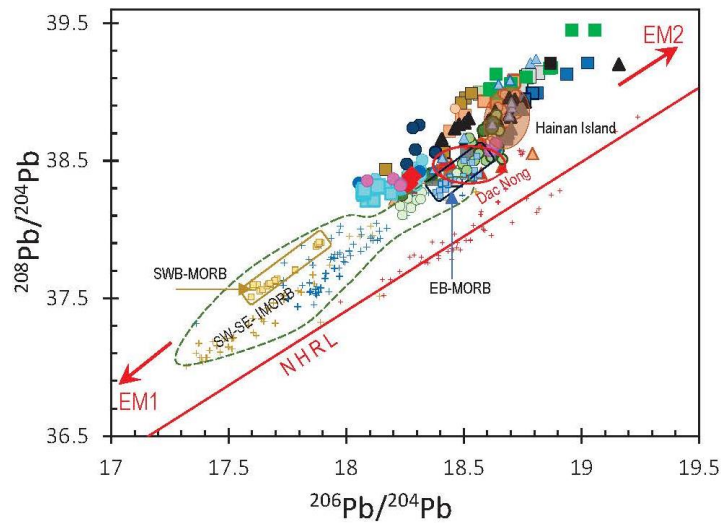


Figure 8b. Correlation between  $^{206}\text{Pb}/^{204}\text{Pb}$  and  $^{208}\text{Pb}/^{204}\text{Pb}$  for post-spreading basalts from Vietnam and neighboring areas. Phu Quy and Ly Son island basalts define low- and high- $^{206}\text{Pb}/^{204}\text{Pb}$  and  $^{208}\text{Pb}/^{204}\text{Pb}$ , respectively. Hainan island basalts form a narrow field with moderately high  $^{206}\text{Pb}/^{204}\text{Pb}$  and  $^{208}\text{Pb}/^{204}\text{Pb}$  compared to many other regional basalts in Indochina. Data sources are as in figure 7. See explanation in the text

Correlation between  $^{206}\text{Pb}/^{204}\text{Pb}$  vs.  $^{207}\text{Pb}/^{204}\text{Pb}$  and  $^{208}\text{Pb}/^{204}\text{Pb}$  for the post-spreading basalt from Vietnam and its neighboring areas (fig. 8a–8b) reveal several particular interesting points as compared to the Sr-Nd isotopic plots. For instance, the East sub-basin (U1431) syn-spreading basalt has a much higher  $^{206}\text{Pb}/^{204}\text{Pb}$  than the SW sub-basin (U1433, U1434). The two fields plot inside the field of SE- and SW-Indian MORB, away from the Pacific -MORB (figs. 8a–8b). Phu Quy island (and Hon Tro)’s basalt defines one of the most radiogenic components in terms of Sr-Nd isotopes (fig. 7), appears one of those lowest  $^{206}\text{Pb}/^{204}\text{Pb}$ , tending strongly to the EM1. The majority of Ly Son basalts, on the other hand, show almost the highest  $^{206}\text{Pb}/^{204}\text{Pb}$ , defining the high end among the post-spreading basalts in Vietnam and its neighboring areas (figs. 8a–8b). Dac Nong and Hainan island basalts trend between the low (Phu Quy) and the high (Ly Son) where Hainan island basalt has higher  $^{206}\text{Pb}/^{204}\text{Pb}$  and  $^{207}\text{Pb}/^{204}\text{Pb}$ , and  $^{208}\text{Pb}/^{204}\text{Pb}$  compared to Dak Nong’s. Note that many old 11-6 Ma basalts have high  $^{207}\text{Pb}/^{204}\text{Pb}$  and  $^{208}\text{Pb}/^{204}\text{Pb}$  relative to  $^{206}\text{Pb}/^{204}\text{Pb}$  compared to Hainan, Dak Nong, and Khorat, suggesting that their mantle sources had higher Th and U

relative to Pb (e.g., White et al., (2010) [55]). In general, the Pb isotopic compositions of the post-spreading basalts in Vietnam and its neighboring areas plot in a triangle with apexes at the depleted mantle (DM, P-MORB) and enriched mantle EM1 and EM2 [57].

Plots of  $^{87}\text{Sr}/^{86}\text{Sr}$  vs.  $^{206}\text{Pb}/^{204}\text{Pb}$  show a clear mixing trend between a depleted mantle and an enriched mantle type 2 (EM2), and to some extent, with an EM1 (fig. 9). From the depleted mantle (DM, I-MORB) moving toward the EM2 include East sub-basin (U1431) syn-spreading basalt, Dac Nong 15-0.2 Ma, Khorat hawaiiite (Thailand 1), Hainan island, almost all the old 11-6 Ma Vietnam basalts along with Bolaven, Khorat basalt (Thailand 2), and Ly Son basalt at the end. In contrast, heading to the EM1 field from a depleted source includes the entire Phu Quy and Hon Tro (IDC) basalt and basalts from SW sub-basin and southeastern regions such as Xuan Loc and Soc Lu (fig. 9). In summary, each syn- and post-EVS spreading basalt area plots to an almost distinctive isotopic field, reflecting space dependence. The isotopic compositions of the basalts exhibit primarily various mixtures of DM and EM2, and to a lesser extent, with EM1 components.

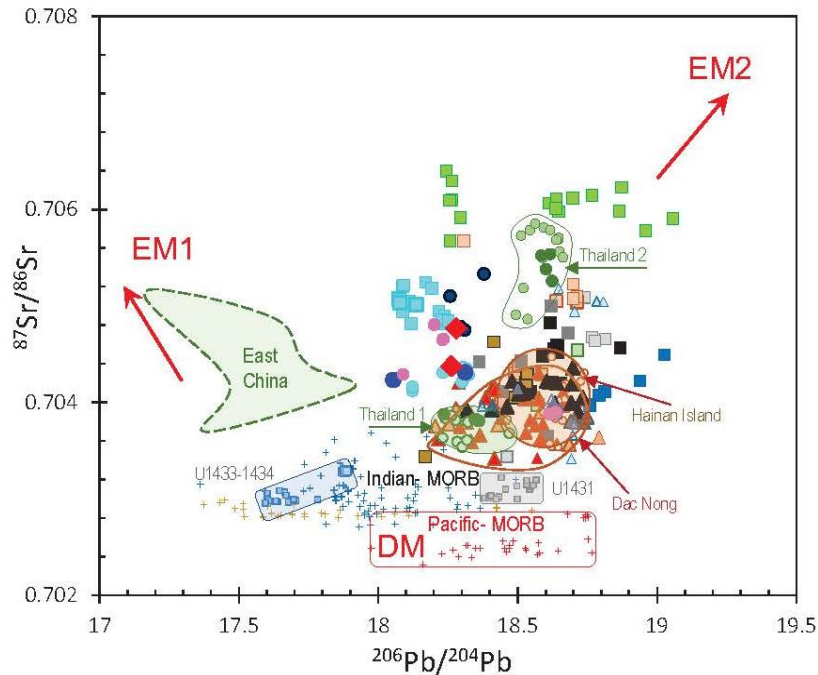


Figure 9. Plots of  $^{87}\text{Sr}/^{86}\text{Sr}$  vs.  $^{206}\text{Pb}/^{204}\text{Pb}$  for post-spreading basalts from Vietnam and neighboring regions. Data sources are as in figure 7. The basalts plot in a triangle defined by DM, EM1 and EM2, reflecting possible mixing among the components. Dak Nong samples are the most depleted and isotopically homogeneous regardless of their various eruption ages (15 to 0.2 Ma). The East China basalt (after [58]) plot in a distinct field, strongly heading to the EM1 field compared to the other regional basalts. See text for explanation

## DISCUSSION

### Geochemistry of mantle source

The geochemical evolution of post-EVS spreading continental basalt and in the EVS basin reveals the general evolutionary trend from basalt tholeiite to alkaline or sub-alkaline basalt [15, 16, 20, 21], suggesting that at least two mantle sources participated in the generation of the magmatic melts and that the melting pressures increased over time. Tejada et al., (2017) [35] studied Re-Os isotope composition on basalt samples from U1431E, U1433B, and U1434 boreholes [20, 21] aged 18, 15 and 12 Ma concluded that at least three different isotope sources involved in the melting to form basaltic melts related to the three above eruptive periods. These researchers suggested that at least two extension phases occurred in the U1431E borehole area. The early controlled the source mixing of an enriched oceanic island basalt and a depleted mid-ocean ridge basalt (OIB-MORB) and the

oceanic crust. The later phase with more enriched Sr, Nd, and Os isotope composition than an enriched (E-) MORB may be derived from the asthenosphere (?).

Qian et al., (2020) studied two volcanic eruption periods of 11-8 Ma and < 8 Ma revealed that the magmas could be classified into two different groups. While the older group (11-8 Ma) has a relatively depleted isotopic and geochemical composition, varying in a narrow range, the younger group (< 8 Ma) has more enriched in Sr and Pb isotope composition that changes in a broader spectrum. The geochemical and isotope composition of the two basalt groups distributed between the enriched (EM2) and the depleted mantle (DM) components, in which the EM2 component influenced the late mantle source more than the early stage. The authors assume that the column melting model is a suitable dynamic to explain the geochemical and isotope composition of the two-phase magma

generation. When the lithosphere is continuously thickened, the mantle melting rate is lower, so the proportion of EM2 joining becomes greater. The researchers suggested that the EM2 component could be introduced into mantle sources eroded from the continental lithosphere [36]. Many authors have reported the trend of basalt evolution in Southeast Asia over time in the context of a similar mantle-lithosphere interaction (e.g., 15-16, 38, 46, 51, 58–61]) to explain the existence of EM1 and EM2 components in basalt.

### Mantle melting

Changes in petrographic-geochemical properties from tholeiite to sub-alkaline or alkaline basalt followed sequentially with fissure eruption patterns forming the volcanic shield, and monogenic stratovolcanoes are widely observed in many basalt centers in Vietnam and neighboring areas [17, 18, 38, 49, 58, 62, 63]. This trend shows that the mantle source composition varies from relatively depleted, heterogeneously depleted to enriched.

The melting pressure calculated using the major element composition showed that tholeiitic basalt melt (early-stage volcanic phase) was generated from 1.2–2 GPa, and late-stage alkaline basalt melt was formed in the range of 2.2–3.2 GPa [38, 64, 65]). The two different melting pressures and geochemical compositions are explained as early magmatic melt formed by spinel-peridotite melting in the lithospheric mantle and the late-stage melt produced by garnet-peridotite from the asthenosphere [38, 61].

Computed melting pressures for Dac Nong tholeiite, sub-alkaline, and Bolaven basalts shows a range from 1.2 GPa to about 2 GPa [48, 51]. This pressure range is also found for old 11-6 Ma basalts from various regions, including Kham Duc, K'Bang, several from Van Hoa, Song Cau, Cung Son, and Phu Quy tholeiites. The basalts with higher computed melting pressures from 2.4 GPa to 3.2 GPa include several Phu Quy and Hon Tro island, and < 1 Ma Trinh Nu and Quang Phu basalts (Dak Nong province) [51, 64, 66].

A garnet-peridotite source melting will form a melt with high LREE such as La, Ce, Nd,... but low HREE like Sm, Ho, Tm, Yb,...

[64], resulting in high LREE/HREE ratios. By contrast, melting a spinel-peridotite produces a melt with a high concentration of the rare earth elements and low LREE/HREE. However, the chondrite normalized rare earth element distribution curves of the representative post-spreading basalts from Vietnam, Bolaven (Southern Laos), Khorat (Thailand), and Hainan island reveal that Hainan basalt has the lowest LREE/HREE, next comes Khorat and Bolaven basalt. In contrast, Vietnam basalt has the highest ratios. This observation suggests that the Hainan island basalts show the most garnet peridotite melting effect among the regional basalts. The Bolaven and Khorat basalts show moderate garnet peridotite influence, whereas Vietnam basalts show the slightest effect. On the one hand, this phenomenon confirms the existence of regional heterogeneity in the melting sources; on the other hand, it may be explained by the interaction of asthenospheric melts with garnet-bearing mafic lenses in the lithosphere mantle or the lower crust during their passage to the surface. The basaltic melt formed by the mixture would also have low HREE composition, thus homogenizing the HREE signature induced by garnet-peridotite melting [46, 53, 67].

### Mantle source heterogeneity

Experimental melting of peridotite and peridotite-pyroxenite hybrid produces basaltic melts with higher FeO, TiO<sub>2</sub>, CaO/Al<sub>2</sub>O<sub>3</sub>, and TiO<sub>2</sub>/Al<sub>2</sub>O<sub>3</sub> with increasing fertility [54, 55]. Among these, melt fractions of the peridotite-pyroxenite mixture are significantly enriched [68, 69] (fig. 5). Correlation between CaO/Al<sub>2</sub>O<sub>3</sub> and TiO<sub>2</sub> is unaffected by fractional crystallization involving (e.g.) olivine, any differences between low- and high-Ti types must reflect factors such as melt temperature, melt fraction, and source fertility [54, 55, 70].

All the Dac Nong old (15.4 Ma) and young (7 Ma to 0.2 Ma) basalts distribute inside the field of experimentally peridotite melt fractions, along with several Vietnam 11-6 Ma samples, Bolaven tholeiite, a few Ly Son and Phu Quy island samples, showing moderate CaO/Al<sub>2</sub>O<sub>3</sub> and low- to high- TiO<sub>2</sub> (fig. 5, field A). These basalts are embedded in-between melt fractions

of moderately fertile (HK-66, line 2) and highly fertile peridotite (PHN 1611, line 4). Since the Dak Nong basalts are mostly aphyric tholeiite and olivine-bearing sub-alkaline basalts, we can assume that the magmas have primarily undergone olivine ± clinopyroxene fractional crystallization. If so, the Dak Nong primitive melts must have a lower TiO<sub>2</sub> and higher CaO/Al<sub>2</sub>O<sub>3</sub> value, supposedly lying between melt fractions of relatively refractory (KLB-1, line 1) and moderately fertile peridotite (HK-66, line 2) (fig. 5). The majority of 2.4-0 Ma Ly Son, Phu Quy, and Hon Tro along with enriched Trinh Nu - Quang Phu, Thong Nhat (Soc Lu) basalts, and Bolaven nephelinite, showing much higher TiO<sub>2</sub> and variable CaO/Al<sub>2</sub>O<sub>3</sub>, are distributed between highly fertile peridotite (line 3) and mixed peridotite - pyroxenite melt fractions (line 4) field (fig. 5, field B). The Khorat samples along with 11-6 Ma Song Cau - Ghenh Da Dia (GDD), Van Hoa - Cung Son have much lower CaO/Al<sub>2</sub>O<sub>3</sub> and high TiO<sub>2</sub>, plotting outside the melt fraction field and reflecting either substantial

olivine and clinopyroxene fractionation or melting from a highly enriched mantle source (fig. 5, field C). Hainan basalt, on the other hand, defines a distinct distribution field in the CaO/Al<sub>2</sub>O<sub>3</sub> - TiO<sub>2</sub> relationship, crossing from field A to the end of field B, mostly separating from all other post-EVS spreading basalts being reported here, suggesting the basaltic melt underwent significant olivine fractionation and or derived from a source different from all other regional post-spreading basalts being mentioned above.

In summary, the post-spreading basalts plot in three separate fields, showing low and high CaO/Al<sub>2</sub>O<sub>3</sub> and variable TiO<sub>2</sub>, suggesting melting from various sources and, or undergoing significant olivine ± clinopyroxene fractional crystallization (fig. 5). Because CaO/Al<sub>2</sub>O<sub>3</sub> ratios and TiO<sub>2</sub> contents depend on the mantle source (fertile vs. refractory), melting temperature, melt fraction, and, to some extent, pressure parameters [54, 55, 68], the geochemical fields suggest the regional heterogeneity in the mantle sources.

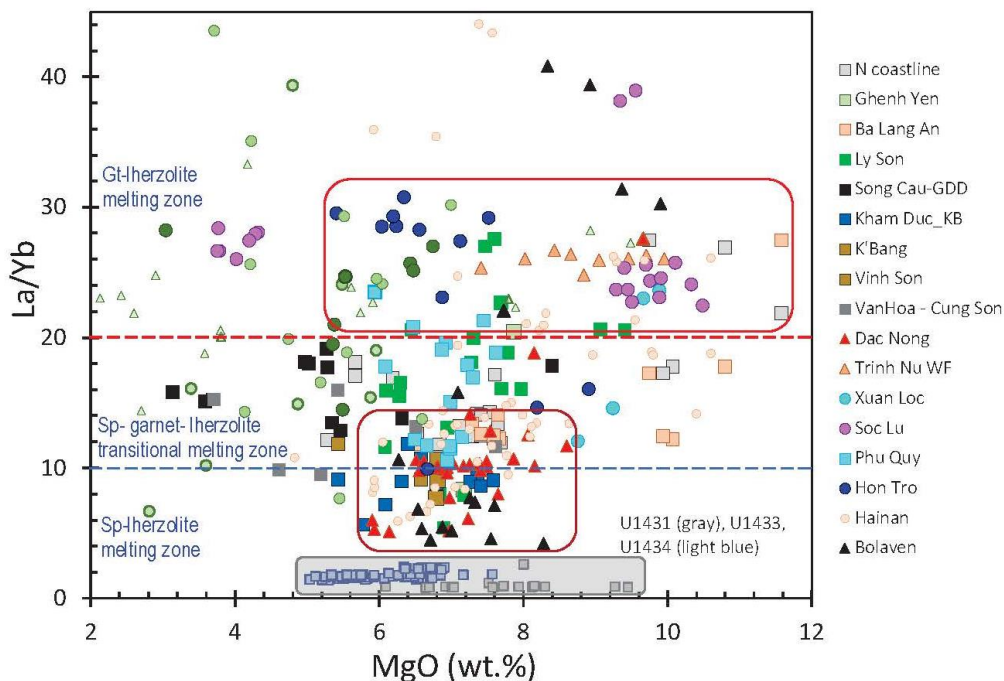


Figure 10. Correlation between MgO and La/Yb for syn- and post-EVS spreading basalts. Melting zones are based on spinel- and garnet-Iherzolite melting modeling [70–72]. Note that just a few of the most isotopically enriched Phu Quy and Ly Son basalts are in the zone of garnet-Iherzolite melting. See text for detail explanations

We have conducted peridotite melting modeling based on the melting parameters and trace element concentrations by Johnson et al., (1990) [71], McKenzie and Bickle (1988) [70], and McKenzie and O’Nions (1991) [72] that shows partial melting 5–10 % of a spinel-lherzolite yields La/Yb ratios varying from 8 to 2. Partial melting from 5–10% of a garnet-lherzolite would yield La/Yb ratios from about 20 to 7. Plots of MgO (wt.%) against La/Yb (fig. 10). As seen in figure 10, isotopically depleted Dak Nong tholeiite, the Bolaven tholeiite and sub-alkaline basalt along with several old 11-6 Ma, and the majority of the Hainan island basalts concentrate in a lower La/Yb ( $< 14$ ) field, most certainly suggesting being derived by spinel lherzolite or spinel-garnet-lherzolite transitional melting. Those of higher La/Yb ( $> 20$ ) possibly produced by garnet lherzolite melting include Hon Tro (IDC), some Khorat and Ly Son island basalt,  $< 1$  Ma Trinh Nu - Quang Phu, Thong Nhat alkaline, and Bolaven nephelinite. Note that most young, enriched EM1-EM2 Ly Son and Phu Quy samples are not in the field of possible garnet-lherzolite melting fields (figs. 7–9). They are not derived from deep levels compared to others (fig. 10).

### Mantle flow model

Several authors have exploited the mantle plume mechanism (e.g., [40, 62, 73, 74] to explain the East Vietnam Sea opening dynamics and associated magma. Hainan mantle plume is not only operational in the opening of the East Vietnam Sea (33-16 Ma) but also the main driver of mantle melting, causing volcanism in the EVS basin (33 Ma - present) and throughout East and Southeast Asia [40, 75, and references therein]. Not to mention the difference in the geochemical (figs. 4–6) and isotopic compositions (figs. 7–9) between the basalt regions believed to have originated from the Hainan mantle plume. Besides, deep seismic data present evidence of an old Pacific subducted plate stagnant in the mantle transition zone (410–660 km) below SE China [76–78], rejecting the idea of a possible mantle plume started from the lower mantle intruding the transition zone to cause the melting in the upper mantle.

Jolivet et al., (2018) [79] synthesize the tectonic studies of Indian plate colliding into Eurasia and its geodynamic consequences such as the formation of intercontinental fault zones, from the Himalayas to the Asian plate margins where the back-arc basin, for example, the Sea of Japan, formed just above the subduction zones of the Pacific and Indian Oceans. However, these authors argue that the role of extrusion and subduction in controlling destruction within the Asian plate at such a long distance (from the impact zone) has not been fully explained. By comparing the plate kinetic orbits and lithospheric blocks 50 million years ago with the mantle flow directions obtained from seismic data, the authors concluded that asthenospheric flows control the connection between the plate extrusion and back-arc opening. This mantle flow originated from the upwelling mantle zone below south Africa, has pushed India more than 3,000 km deep into Asia from the beginning of the drift. The mantle flow then intrudes Asia as far as oceanic trenches in the east and southeast, leading to subducted slab roll-back, forming the shape and dynamics of regional faults and back-arcs. The authors suggested that the continental deformation by the asthenospheric flows provided a different view on the process of continental destruction and arose a new research direction on the mantle dynamics below the continent in the past [79].

The work of Jolivet et al., (2018) [79] has several conclusions about the deformation of Asia from the time India began to collide and extrude Asia about 50 million years ago as follows: The Asian deformation is driven by (1) asthenosphere flow originating from anomalous low-velocity regions below the south and west Africa and the southwest Indian Ocean reaching as far as back-arc regions in the Western Pacific, (2) the compression initiated from the continent-continent collision zones in the lithosphere, and by (3) the plate roll-back to the east and southeast from the collision zone.

A shallower mantle flow resulting from transversal transitions stemming from a continent collision in the Himalayas and the ocean subduction in the Sunda trench creates a southward flow associated with the Sunda

trench retreat. Combining the two mantle flows leads to the opening of back-arc basins such as the Sea of Japan and the East Vietnam Sea, controlled by the large-scale right and left slip fault zones. The main shortening direction in continental deformation, between the impact site and the subduction zone of the Pacific Ocean, in this case, can be considered as the flow direction in the below asthenosphere, and it can become a valuable tool for evaluating the mantle flow below continents in the past [79].

#### **The East Vietnam Sea opening tectonics, induced magma and the role of mantle flow**

Volcanic eruptions in the deep EVS basin, on the Vietnam continent, and in Southeast Asia, in general, are believed to relate to the lithosphere extension by deep fault systems [80] combined with the mantle upwelling that followed the Tethys Sea closure due to the collision of the Indian plate into Eurasia [38, 41, 45, 64, 79, 81].

The decompression melting of mantle material occurs typically due to extension tectonic activities, appearing on a large scale and having a profound influence on the lithospheric mantle layer. There are two general lithosphere stretching types: Uniform stretching and shear stretching [28]. The extension intensity is determined by the extension coefficient  $\beta$ , which is the crustal thickness ratio before and after the extension. Under normal mantle heat (1,280°C), decompression melting is possible only if  $\beta > 2.8$ , but with normal mantle heat, the shear stretching cannot cause depressurized melting [28]. Under higher-than-normal mantle thermal conditions, assuming 1,480°C; uniform lithosphere extension can cause depressurized melting with a coefficient  $\beta$  just  $> 1.5$  (compared with shear stretching of 4).

Seismic data and deep-sea borehole records in the East Vietnam Sea along, or nearby, the old oceanic spreading axis detect basalt layers and volcanoclastic sediments simultaneously with East Vietnam Sea opening tectonics ( $> 16$  Ma) [20, 21, 26, 27] (fig. 1). However, the appearance of syn-EVS spreading magmas is not regular, continuous, and voluminous, only corresponding to the scale of the slow to medium oceanic spreading

rate (20–35 km/million years) [26, 27]; although somewhere, the EVS spreading is rapid, up to 70–80 km/million year [20]. Studying in detail the seismic stratigraphy and magma occurrence in the Southwestern sub-basin of the East Vietnam Sea about 10 million years after the cessation of EVS opening, Li et al., (2013) [80] believed that the magma does not have a clear relationship with the regional tectonic activity. With the extension faults detected in the area, these authors confirm that their extension rate is far from reaching a coefficient of  $\beta > 2.8$  to cause melting of a mantle source at average temperature (about 1,280°C). Consequently, Li et al., (2013) [80] conclude that the asthenosphere mechanism rather than the lithosphere is the cause of melting and magmatism in the Southwestern sub-basin [20, 80].

#### **CONCLUSIONS**

From the above discussions, we come to the following conclusions:

1. East Vietnam (South China) Sea opening occurred from 33 Ma to 16-15.5 Ma, accompanied by basaltic eruptions under the mantle-decompression melting mechanism simultaneously with the oceanic crust spreading. Post-EVS spreading volcanic eruption ( $< 16$ -0 Ma) is widespread in the EVS basin and extends to South and Southeast China, Hainan island, Southern Laos, Thailand, and many parts of the continent, coastal and shelf areas of Vietnam.

2. The syn-EVS spreading basalt is geochemically depleted, similar to the mid-ocean ridge basalt (MORB), vastly different from the typical enriched intraplate basalt (OIB-type). The post-EVS spreading magma in Vietnam, Southern Laos, Thailand, and Hainan island consists of alkaline basalt, sub-alkali, and tholeiite, with different rare earth elemental geochemistry properties that reflect the melting source transition from spinel peridotite to garnet peridotite over time.

3. The Sr-Nd-Pb isotopic compositions of the post-spreading regional basalts are strongly heterogeneous, distributed between the depleted mantle (DM) and the enriched mantle (EM1, EM2) components, reflecting the mixing

process of their asthenosphere-derived melts with the lithospheric mantle or crustal material on their passage to the surface.

4. The geochemical and isotopic compositions of the regional post-EVS spreading basalts in Vietnam, Laos, and Thailand plot to different fields regardless of eruption ages, implying space dependence. Thus, it is impossible to explain their formation by a single mechanism such as a deep-seated mantle plume.

5. The consequences of displacement dynamics of the mantle flow originating from the thermally anomalous region below the south and west Africa and the central Indian Ocean run as far as the back-arc basins in the Western Pacific lead to continent-continent collisions, opening the marginal sea, rolling back the subduction plate east and southeast, and induce upper mantle decompression melting [79, 81].

**Acknowledgments:** Boloven basalt sampling was partially funded by the Vietnam Academy of Science and Technology to project coded QTLA01/21–22, the Institute of Geological Sciences supported the 2020 Basic Research project to the Center of Analytical Laboratories. The National Science and Technology Project financed the study coded KC.09.31/16–20. The authors are gratefully acknowledged for their support.

Supplementary data may be found in Appendix A.

## REFERENCES

- [1] Leloup, P. H., Arnaud, N., Lacassin, R., Kienast, J. R., Harrison, T. M., Trong, T. P., Replumaz, A., and Tapponnier, P., 2001. New constraints on the structure, thermochronology, and timing of the Ailao Shan-Red River shear zone, SE Asia. *Journal of Geophysical Research: Solid Earth*, 106(B4), 6683–6732. <https://doi.org/10.1029/2000JB900322>
- [2] Tapponnier, P., Peltzer, G., and Armijo, R., 1986. On the mechanics of the collision between India and Asia. *Geological Society, London, Special Publications*, 19(1), 113–157. <https://doi.org/10.1144/GSL.SP.1986.019.01.07>
- [3] Tapponnier, P., Peltzer, G. L. D. A. Y., Le Dain, A. Y., Armijo, R., and Cobbold, P., 1982. Propagating extrusion tectonics in Asia: New insights from simple experiments with plasticine. *Geology*, 10(12), 611–616. [https://doi.org/10.1130/0091-7613\(1982\)10<611:PETIAN>2.0.CO;2](https://doi.org/10.1130/0091-7613(1982)10<611:PETIAN>2.0.CO;2)
- [4] Taylor, B., and Hayes, D. E., 1983. Origin and history of the South China Sea basin. *Washington DC American Geophysical Union Geophysical Monograph Series*, 27, 23–56. doi: 10.1029/GM027p0023
- [5] Briais, A., Patriat, P., and Tapponnier, P., 1993. Updated interpretation of magnetic anomalies and seafloor spreading stages in the South China Sea: Implications for the Tertiary tectonics of Southeast Asia. *Journal of Geophysical Research: Solid Earth*, 98(B4), 6299–6328. <https://doi.org/10.1029/92JB02280>
- [6] Barckhausen, U., Engels, M., Franke, D., Ladage, S., and Pubellier, M., 2014. Evolution of the South China Sea: Revised ages for breakup and seafloor spreading. *Marine and Petroleum Geology*, 58, 599–611. <https://doi.org/10.1016/j.marpetgeo.2014.02.022>
- [7] Rangin, C., Huchon, P., Le Pichon, X., Bellon, H., Lepvrier, C., Roques, D., Heo, N. D., and Van Quynh, P., 1995. Cenozoic deformation of central and south Vietnam. *Tectonophysics*, 251(1-4), 179–196. [https://doi.org/10.1016/0040-1951\(95\)00006-2](https://doi.org/10.1016/0040-1951(95)00006-2)
- [8] Clift, P., Lee, G. H., Anh Duc, N., Barckhausen, U., van Long, H., and Zhen, S., 2008. Seismic reflection evidence for a Dangerous Grounds miniplate: No extrusion origin for the South China Sea. *Tectonics*, 27(3), TC3008. doi: 10.1029/2007TC002216
- [9] Shi, H., and Li, C. F., 2012. Mesozoic and early Cenozoic tectonic convergence-to-rifting transition prior to opening of the South China Sea. *International Geology Review*, 54(15), 1801–1828.

- <https://doi.org/10.1080/00206814.2012.677136>
- [10] Hayes, D. E., and Nissen, S. S., 2005. The South China sea margins: Implications for rifting contrasts. *Earth and Planetary Science Letters*, 237(3–4), 601–616. <https://doi.org/10.1016/j.epsl.2005.06.017>
- [11] Pautot, G., and Rangin, C., 1989. Subduction of the South China Sea axial ridge below Luzon (Philippines). *Earth and Planetary Science Letters*, 92(1), 57–69. [https://doi.org/10.1016/0012-821X\(89\)90020-4](https://doi.org/10.1016/0012-821X(89)90020-4)
- [12] Ru, K., and Pigott, J. D., 1986. Episodic rifting and subsidence in the South China Sea. *AAPG bulletin*, 70(9), 1136–1155. <https://doi.org/10.1306/94886A8D-1704-11D7-8645000102C1865D>
- [13] Hall, R., 1996. Reconstructing Cenozoic SE Asia. *Geological Society, London, Special Publications*, 106(1), 153–184. <https://doi.org/10.1144/GSL.SP.1996.106.01.11>
- [14] Lee, T. Y., Lo, C. H., Chung, S. L., Chen, C. Y., Wang, P. L., Lin, W. P., Hoang, N., Chi, C. T., and Yem, N. T., 1998. <sup>40</sup>Ar/<sup>39</sup>Ar dating result of Neogene basalts in Vietnam and its tectonic implication. *Mantle Dynamics and Plate Interactions in East Asia*, 27, 317–330. <https://doi.org/10.1029/GD027p0317>
- [15] Tu, K., Flower, M. F., Carlson, R. W., Zhang, M., and Xie, G., 1991. Sr, Nd, and Pb isotopic compositions of Hainan basalts (south China): implications for a subcontinental lithosphere Dupal source. *Geology*, 19(6), 567–569. [https://doi.org/10.1130/0091-7613\(1991\)019<0567:SNAPIC>2.3.CO;2](https://doi.org/10.1130/0091-7613(1991)019<0567:SNAPIC>2.3.CO;2)
- [16] Tu, K., Flower, M. F., Carlson, R. W., Xie, G., Chen, C. Y., and Zhang, M., 1992. Magmatism in the South China Basin: 1. Isotopic and trace-element evidence for an endogenous Dupal mantle component. *Chemical Geology*, 97(1–2), 47–63. [https://doi.org/10.1016/0009-2541\(92\)90135-R](https://doi.org/10.1016/0009-2541(92)90135-R)
- [17] Ho, K. S., Chen, J. C., and Juang, W. S., 2000. Geochronology and geochemistry of late Cenozoic basalts from the Leiqiong area, southern China. *Journal of Asian Earth Sciences*, 18(3), 307–324. [https://doi.org/10.1016/S1367-9120\(99\)00059-0](https://doi.org/10.1016/S1367-9120(99)00059-0)
- [18] Yan, P., Deng, H., Liu, H., Zhang, Z., and Jiang, Y., 2006. The temporal and spatial distribution of volcanism in the South China Sea region. *Journal of Asian Earth Sciences*, 27(5), 647–659. <https://doi.org/10.1016/j.jseaes.2005.06.005>
- [19] Yan, Q., Shi, X., Wang, K., Bu, W., and Xiao, L., 2008. Major element, trace element, and Sr, Nd and Pb isotope studies of Cenozoic basalts from the South China Sea. *Science in China Series D: Earth Sciences*, 51(4), 550–566. doi: 10.1007/s11430-008-0026-3
- [20] Li, C. F., Xu, X., Lin, J., Sun, Z., Zhu, J., Yao, Y., Zhao, X., Liu, Q., Kulhanek, D. K., Wang, J., Song, T., Zhao, J., Qiu, N., Guan, Y., Zhou, Z., Williams, T., Bao, R., Briais, A., Brown, E. A., Chen, Y., Clift, P. D., Colwell, F. S., Dadd, K. A., Ding, W., Almeida, I. H., Huang, X. L., Hyun, S., Jiang, T., Koppers, A. A. P., Li, Q., Liu, C., Liu, Z., Nagai, R. H., Peleolampay, A., Su, X., Tejada, M. L. G., Trinh, H. S., Yeh, Y. C., Zhang, C., Zhang, F., and Zhang, G. L., 2014. Ages and magnetic structures of the South China Sea constrained by deep tow magnetic surveys and IODP Expedition 349. *Geochemistry, Geophysics, Geosystems*, 15(12), 4958–4983. <https://doi.org/10.1002/2014GC005567>
- [21] Li, C. F., Lin, J., and Kulhanek, D. K., 2015. the Expedition 349 Scientists. 2015b. *Proceedings of the International Ocean Discovery Program*, 349, 1–43.
- [22] Tamaki, K., 1988. Geological structures of the Japan sea and its tectonic implications. *Bulletin of the Geological Survey of Japan*, 39, 269–365.
- [23] Kimura, G., and Tamaki, K., 1986. Collision, rotation, and back-arc spreading in the region of the Okhotsk and Japan Seas. *Tectonics*, 5(3), 389–401. doi: 10.1029/TC005i003p00389
- [24] Jolivet, L., Tamaki, K., and Fournier, M., 1994. Japan Sea, opening history and

- mechanism: A synthesis. *Journal of Geophysical Research: Solid Earth*, 99(B11), 22237–22259. <https://doi.org/10.1029/93JB03463>
- [25] Kaneoka, I., Notsu, K., Takigami, Y., Fujioka, K., and Sakai, H., 1990. Constraints on the evolution of the Japan Sea based on  $^{40}\text{Ar}$ - $^{39}\text{Ar}$  ages and Sr isotopic ratios for volcanic rocks of the Yamato Seamount chain in the Japan Sea. *Earth and Planetary Science Letters*, 97(1–2), 211–225. [https://doi.org/10.1016/0012-821X\(90\)90109-B](https://doi.org/10.1016/0012-821X(90)90109-B)
- [26] Sun, Z., Jian, Z., Stock, J. M., Larsen, H. C., Klaus, A., Alvarez Zarikian, C. A., Boaga, J., Bowden, S. A., Briaies, A., Chen, Y., Cukur, D., Dadd, K. A., Ding, W., Dorais, M. J., Ferré, E. C., Ferreira, F., Furusawa, A., Gewecke, A. J., Hinojosa, J. L., Höfig, T. W., Hsiung, K. H., Huang, B., Huang, E., Huang, X. L., Jiang, S., Jin, H., Johnson, B. G., Kurzwski, R. M., Lei, C., Li, B., Li, L., Li, Y., Lin, J., Liu, C., Liu, C., Liu, Z., Luna, A., Lupi, C., McCarthy, A. J., Mohn, G., Ningthoujam, L. S., Nirrengarten, M., Osono, N., Peate, D. W., Persaud, P., Qiu, N., Robinson, C. M., Satolli, S., Sauermilch, I., Schindlbeck, J. C., Skinner, S. M., Straub, S. M., Su, X., Tian, L., van der Zwan, F. M., Wan, S., Wu, H., Xiang, R., Yadav, R., Yi, L., Zhang, C., Zhang, J., Zhang, Y., Zhao, N., Zhong, G., and Zhong, L., 2018. Expedition 367/368 methods. *Sun, Z., Jian, Z., Stock, JM, Larsen, HC, Klaus, A., Alvarez Zarikian, CA, and the Expedition, 367, 368.* <https://doi.org/10.14379/iodp.proc.367368.102.2018>
- [27] Larsen, H. C., Mohn, G., Nirrengarten, M., Sun, Z., Stock, J., Jian, Z., Klaus, A., Alvarez-Zarikian, C. A., Boaga, J., Bowden, S. A., Briaies, A., Chen, Y., Cukur, D., Dadd, K., Ding, W., Dorais, M., Ferré, E. C., Ferreira, F., Furusawa, A., Gewecke, A., Hinojosa, J., Höfig, T. W., Hsiung, K. H., Huang, B., Huang, E., Huang, X. L., Jiang, S., Jin, H., Johnson, B. G., Kurzwski, R. M., Lei, C., Li, B., Li, L., Li, Y., Lin, J., Liu, C., Liu, C., Liu, Z., Luna, A. J., Lupi, C., McCarthy, A., Ningthoujam, L., Osono, N., Peate, D. W., Persaud, P., Qiu, N., Robinson, C., Satolli, S., Sauermilch, I., Schindlbeck, J. C., Skinner, S., Straub, S., Su, X., Su, C., Tian, L., van der Zwan, F. M., Wan, S., Wu, H., Xiang, R., Yadav, R., Yi, L., Yu, P. S., Zhang, C., Zhang, J., Zhang, Y., Zhao, N., Zhong, G., and Zhong, L., 2018. Rapid transition from continental breakup to igneous oceanic crust in the South China Sea. *Nature Geoscience*, 11(10), 782–789. <https://doi.org/10.1038/s41561-018-0198-1>
- [28] Latin, D., and White, N., 1990. Generating melt during lithospheric extension: Pure shear vs. simple shear. *Geology*, 18(4), 327–331. [https://doi.org/10.1130/0091-7613\(1990\)018<0327:GMDLEP>2.3.CO;2](https://doi.org/10.1130/0091-7613(1990)018<0327:GMDLEP>2.3.CO;2)
- [29] White, W. M., Hofmann, A. W., and Puchelt, H., 1987. Isotope geochemistry of Pacific mid-ocean ridge basalt. *Journal of Geophysical Research: Solid Earth*, 92(B6), 4881–4893. <https://doi.org/10.1029/JB092iB06p04881>
- [30] Mahoney, J. J., 1988. Deccan traps. In *Continental flood basalts* (pp. 151–194). Springer, Dordrecht. doi: 10.1007/978-94-015-7805-9\_5
- [31] Mahoney, J. J., Graham, D. W., Christie, D. M., Johnson, K. T. M., Hall, L. S., and Vonderhaar, D. L., 2002. Between a hotspot and a cold spot: isotopic variation in the Southeast Indian Ridge asthenosphere, 86°E–118°E. *Journal of Petrology*, 43(7), 1155–1176. doi: 10.1093/petrology/43.7.1155
- [32] Neal, C. R., Mahoney, J. J., and Chazey III, W. J., 2002. Mantle sources and the highly variable role of continental lithosphere in basalt petrogenesis of the Kerguelen Plateau and Broken Ridge LIP: Results from ODP Leg 183. *Journal of Petrology*, 43(7), 1177–1205. doi: 10.1093/petrology/43.7.1177
- [33] Wang, X. J., Wu, M. Q., Liang, D. H., and Yin, A. W., 1984. Some geochemical characteristics of basalts in the South China Sea. *Geochimica*, (4), 332–340.

- [34] Zou, H., Zindler, A., Xu, X., and Qi, Q., 2000. Major, trace element, and Nd, Sr and Pb isotope studies of Cenozoic basalts in SE China: mantle sources, regional variations, and tectonic significance. *Chemical Geology*, 171(1-2), 33-47. [https://doi.org/10.1016/S0009-2541\(00\)00243-6](https://doi.org/10.1016/S0009-2541(00)00243-6)
- [35] Tejada, M. L. G., Castillo, P., Huang, X. L., and Senda, R., 2017. Geochemistry of the South China Sea basalts. *IODP Expedition 349. 3100 Goldschmidt Conference Abstracts Paris Aug. 2017*.
- [36] Qian, S., Zhou, H., Zhang, L., and Cheng, R., 2020. Mantle heterogeneity beneath the South China Sea: Chemical and isotopic evidence for contamination of ambient asthenospheric mantle. *Lithos*, 354, 105335. <https://doi.org/10.1016/j.lithos.2019.105335>
- [37] Flower, M. F., Zhang, M., Chen, C. Y., Tu, K., and Xie, G., 1992. Magmatism in the south China basin: 2. Post-spreading Quaternary basalts from Hainan Island, south China. *Chemical Geology*, 97(1-2), 65-87. [https://doi.org/10.1016/0009-2541\(92\)90136-S](https://doi.org/10.1016/0009-2541(92)90136-S)
- [38] Hoang, N., and Flower, M., 1998. Petrogenesis of Cenozoic basalts from Vietnam: implication for origins of a 'diffuse igneous province'. *Journal of Petrology*, 39(3), 369-395. <https://doi.org/10.1093/petroj/39.3.369>
- [39] Wang, X. C., Li, Z. X., Li, X. H., Li, J., Liu, Y., Long, W. G., Zhou, J. B., and Wang, F., 2012. Temperature, pressure, and composition of the mantle source region of Late Cenozoic basalts in Hainan Island, SE Asia: a consequence of a young thermal mantle plume close to subduction zones?. *Journal of Petrology*, 53(1), 177-233. <https://doi.org/10.1093/petrology/egr061>
- [40] Yan, Q., Shi, X., Metcalfe, I., Liu, S., Xu, T., Kornkanitnan, N., Sirichaiseth, T., Yuan, L., Zhang, Y., and Zhang, H., 2018. Hainan mantle plume produced late Cenozoic basaltic rocks in Thailand, Southeast Asia. *Scientific Reports*, 8(1), 1-14. <https://doi.org/10.1038/s41598-018-20712-7>
- [41] Wang, J. H., Yin, A., Harrison, T. M., Grove, M., Zhang, Y. Q., and Xie, G. H., 2001. A tectonic model for Cenozoic igneous activities in the eastern Indo-Asian collision zone. *Earth and Planetary Science Letters*, 188(1-2), 123-133. doi: 10.1016/S0012-821X(01)00315-6
- [42] Hoang, N., Huong, T. T., and Anh, L. D., 2019. Geochemistry and petrology of spinel-lherzolite xenoliths in Cenozoic alkaline basalt in Vietnam: implications for lithospheric mantle source domain. *Geology and Metallogeny of Vietnam, Int Symposium, Hanoi March 2019*, pp. 77-94, ISBN 978-604-913-809-6.
- [43] Ignat'ev, A. V., Velivetskaya, T. A., and Budnitskii, S. Y., 2010. A method for determining argon isotopes in a continuous helium flow for K/Ar geochronology. *Journal of Analytical Chemistry*, 65(13), 1347-1355. doi: 10.1134/S1061934810130071
- [44] Bui Thi Sinh, V., Osanai, Y., Lenz, C., Nakano, N., Adachi, T., Belousova, E., and Kitano, I., 2019. Gem-quality zircon megacrysts from placer deposits in the central highlands, Vietnam-potential source and links to Cenozoic Alkali Basalts. *Minerals*, 9(2), 89. <https://doi.org/10.3390/min9020089>
- [45] Hoang, N., and Uto, K., 2006. Upper mantle isotopic components beneath the Ryukyu arc system: Evidence for 'back-arc' entrapment of Pacific MORB mantle. *Earth and Planetary Science Letters*, 249(3-4), 229-240. <https://doi.org/10.1016/j.epsl.2006.07.021>
- [46] Hoang, N., Shinjo, R., Huong, T. T., Pécskay, Z., and Bac, D. T., 2019. Pleistocene basaltic volcanism in the Krông Nô area and vicinity, Dak Nong province (Vietnam). *Journal of Asian Earth Sciences*, 181, 103903. doi: 10.1016/j.jseae.2019.103903
- [47] Zhang, G. L., Luo, Q., Zhao, J., Jackson, M. G., Guo, L. S., and Zhong, L. F., 2018. Geochemical nature of sub-ridge mantle and opening dynamics of the South China

- Sea. *Earth and Planetary Science Letters*, 489, 145–155. <https://doi.org/10.1016/j.epsl.2018.02.040>
- [48] Hoang, N., Hauzenberger, C., Fukuyama, M., and Konzett, J., 2018. Cenozoic volcanism in the Bolaven, Southern Laos. *25<sup>th</sup> GEOSEA 2018, Hanoi, 16–17 October 2018*, pp. 97–98.
- [49] Zhou, P., and Mukasa, S. B., 1997. Nd-Sr-Pb isotopic, and major-and trace-element geochemistry of Cenozoic lavas from the Khorat Plateau, Thailand: sources and petrogenesis. *Chemical Geology*, 137(3–4), 175–193. doi: 10.1016/S0009-2541(96)00162-3
- [50] Hoang, N., Flower, M. F., and Carlson, R. W., 1996. Major, trace element, and isotopic compositions of Vietnamese basalts: interaction of hydrous EM1-rich asthenosphere with thinned Eurasian lithosphere. *Geochimica et cosmochimica Acta*, 60(22), 4329–4351. [https://doi.org/10.1016/S0016-7037\(96\)00247-5](https://doi.org/10.1016/S0016-7037(96)00247-5)
- [51] Hoàng, N., Flower, M. F., Xuân, P. T., Quý, H. V., and Sơn, T. T., 2013. Collision-induced basalt eruptions at Pleiku and Buôn Mê Thuột, south-central Viet Nam. *Journal of Geodynamics*, 69, 65–83. <https://doi.org/10.1016/j.jog.2012.03.012>
- [52] Holm, P. M., 2002. Sr, Nd and Pb isotopic composition of in situ lower crust at the Southwest Indian Ridge: results from ODP Leg 176. *Chemical Geology*, 184(3–4), 195–216. [https://doi.org/10.1016/S0009-2541\(01\)00364-3](https://doi.org/10.1016/S0009-2541(01)00364-3)
- [53] Hoang, T. H. A., Choi, S. H., Yu, Y., Pham, T. H., Nguyen, K. H., and Ryu, J. S., 2018. Geochemical constraints on the spatial distribution of recycled oceanic crust in the mantle source of late Cenozoic basalts, Vietnam. *Lithos*, 296, 382–395. <https://doi.org/10.1016/j.lithos.2017.11.020>
- [54] Hirose, K., and Kushiro, I., 1993. Partial melting of dry peridotites at high pressures: determination of compositions of melts segregated from peridotite using aggregates of diamond. *Earth and Planetary Science Letters*, 114(4), 477–489. [https://doi.org/10.1016/0012-821X\(93\)90077-M](https://doi.org/10.1016/0012-821X(93)90077-M)
- [55] Kushiro, I., 1996. Partial melting of fertile mantle peridotite at high pressures: an experimental study using aggregates of diamond. *Geophysical Monograph-American Geophysical Union*, 95, 109–122.
- [56] Sun, S. S., and McDonough, W. F., 1989. Chemical and isotopic systematics of oceanic basalts: implications for mantle composition and processes. *Geological Society, London, Special Publications*, 42(1), 313–345. <https://doi.org/10.1144/GSL.SP.1989.042.01.19>
- [57] Zindler, A., and Hart, S., 1986. Chemical geodynamics. *Annual Review of Earth and Planetary Sciences*, 14(1), 493–571. <https://doi.org/10.1146/annurev.ea.14.050186.002425>
- [58] Tatsumoto, M., Basu, A. R., Wankang, H., Junwen, W., and Guanghong, X., 1992. Sr, Nd, and Pb isotopes of ultramafic xenoliths in volcanic rocks of Eastern China: enriched components EM1 and EM2 in subcontinental lithosphere. *Earth and Planetary Science Letters*, 113(1–2), 107–128. [https://doi.org/10.1016/0012-821X\(92\)90214-G](https://doi.org/10.1016/0012-821X(92)90214-G)
- [59] White, W. M., 2010. Oceanic island basalts and mantle plumes: the geochemical perspective. *Annual Review of Earth and Planetary Sciences*, 38, 133–160. <https://doi.org/10.1146/annurev-earth-040809-152450>
- [60] Tuzo Wilson, J., 1963. Hypothesis of earth's behaviour. *Nature*, 198(4884), 925–929. doi: 10.1038/198925a0
- [61] Hoang, N., and Uto, K., 2003. Geochemistry of Cenozoic basalts in the Fukuoka district (northern Kyushu, Japan): implications for asthenosphere and lithospheric mantle interaction. *Chemical Geology*, 198(3–4), 249–268. doi: 10.1016/S0009-2541(03)00031-7
- [62] Hui, G., Li, S., Li, X., Guo, L., Suo, Y., Somerville, I. D., Zhao, S., Hu, M., Lan, H., and Zhang, J., 2016. Temporal and spatial distribution of Cenozoic igneous rocks in the South China Sea and its adjacent regions: Implications for

- tectono-magmatic evolution. *Geological Journal*, 51, 429–447. <https://doi.org/10.1002/gj.2801>
- [63] Sun, P., Niu, Y., Guo, P., Chen, S., Duan, M., Gong, H., Wang, X., and Xiao, Y., 2019. Multiple mantle metasomatism beneath the Leizhou Peninsula, South China: evidence from elemental and Sr-Nd-Pb-Hf isotope geochemistry of the late Cenozoic volcanic rocks. *International Geology Review*, 61(14), 1768–1785. <https://doi.org/10.1080/00206814.2018.1548307>
- [64] Hoang, N., Shakirov, R. B., and Huong, T. T., 2017. Geochemistry of late miocene-pleistocene basalts in the Phu Quy island area (East Vietnam Sea): Implication for mantle source feature and melt generation. *Vietnam Journal of Earth Sciences*, 39(3), 270–288. <https://doi.org/10.15625/0866-7187/39/3/10559>
- [65] Putirka, K. D., Perfit, M., Ryerson, F. J., and Jackson, M. G., 2007. Ambient and excess mantle temperatures, olivine thermometry, and active vs. passive upwelling. *Chemical Geology*, 241(3–4), 177–206. <https://doi.org/10.1016/j.chemgeo.2007.01.014>
- [66] Anh, L. D., Hoang, N., Phung, V. P., Malinovskii, A. I., Dinh, Q. S., and Shakirov, R. B., 2019. Geochemical features of olivines from Northeastern Phu Quy volcanic island and their relation to melt variations in the magma source. *Journal of Geology*, series B, (49-50), 1–18.
- [67] Robinson, J. A. C., and Wood, B. J., 1998. The depth of the spinel to garnet transition at the peridotite solidus. *Earth and Planetary Science Letters*, 164(1–2), 277–284. [https://doi.org/10.1016/S0012-821X\(98\)00213-1](https://doi.org/10.1016/S0012-821X(98)00213-1)
- [68] Kogiso, T., Hirose, K., and Takahashi, E., 1998. Melting experiments on homogeneous mixtures of peridotite and basalt: application to the genesis of ocean island basalts. *Earth and Planetary Science Letters*, 162(1–4), 45–61. [https://doi.org/10.1016/S0012-821X\(98\)00156-3](https://doi.org/10.1016/S0012-821X(98)00156-3)
- [69] Heinonen, J. S., Luttinen, A. V., Riley, T. R., and Michallik, R. M., 2013. Mixed pyroxenite–peridotite sources for mafic and ultramafic dikes from the Antarctic segment of the Karoo continental flood basalt province. *Lithos*, 177, 366–380. <https://doi.org/10.1016/j.lithos.2013.05.015>
- [70] Mckenzie, D. A. N., and Bickle, M. J., 1988. The volume and composition of melt generated by extension of the lithosphere. *Journal of petrology*, 29(3), 625–679. <https://doi.org/10.1093/petrology/29.3.625>
- [71] Johnson, K. T., Dick, H. J., and Shimizu, N., 1990. Melting in the oceanic upper mantle: an ion microprobe study of diopsides in abyssal peridotites. *Journal of Geophysical Research: Solid Earth*, 95(B3), 2661–2678. <https://doi.org/10.1029/JB095iB03p02661>
- [72] McKenzie, D. A. N., and O’niions, R. K., 1991. Partial melt distributions from inversion of rare earth element concentrations. *Journal of Petrology*, 32(5), 1021–1091. <https://doi.org/10.1093/petrology/32.5.1021>
- [73] Li, N., Yan, Q., Chen, Z., and Shi, X., 2013. Geochemistry and petrogenesis of Quaternary volcanism from the islets in the eastern Beibu Gulf: evidence for Hainan plume. *Acta Oceanologica Sinica*, 32(12), 40–49. <https://doi.org/10.1007/s13131-013-0386-1>
- [74] Yang, F., Huang, X. L., Xu, Y. G., and He, P. L., 2019. Plume-ridge interaction in the South China Sea: Thermometric evidence from Hole U1431E of IODP Expedition 349. *Lithos*, 324, 466–478. <https://doi.org/10.1016/j.lithos.2018.11.031>
- [75] Xu, Y., Wei, J., Qiu, H., Zhang, H., and Huang, X., 2012. Opening and evolution of the South China Sea constrained by studies on volcanic rocks: Preliminary results and a research design. *Chinese Science Bulletin*, 57(24), 3150–3164. <https://doi.org/10.1007/s11434-011-4921-1>

- [76] Káráson, H., and Van Der Hilst, R. D., 2000. Constraints on mantle convection from seismic tomography. *Washington DC American Geophysical Union Geophysical Monograph Series*, 121, 277–288. doi: 10.1029/GM121p0277
- [77] Schellart, W. P., Chen, Z., Strak, V., Duarte, J. C., and Rosas, F. M., 2019. Pacific subduction control on Asian continental deformation including Tibetan extension and eastward extrusion tectonics. *Nature communications*, 10(1), 1–15. <https://doi.org/10.1038/s41467-019-12337-9>
- [78] Zhao, D., Toyokuni, G., and Kurata, K., 2021. Deep mantle structure and origin of Cenozoic intraplate volcanoes in Indochina, Hainan and South China Sea. *Geophysical Journal International*, 225(1), 572–588. <https://doi.org/10.1093/gji/ggaa605>
- [79] Jolivet, L., Faccenna, C., Becker, T., Tesauro, M., Sternai, P., and Bouilhol, P., 2018. Mantle flow and deforming continents: From India-Asia convergence to Pacific subduction. *Tectonics*, 37(9), 2887–2914. <https://doi.org/10.1029/2018TC005036>
- [80] Li, L., and Clift, P. D., 2013. The sedimentary, magmatic and tectonic evolution of the southwestern South China Sea revealed by seismic stratigraphic analysis. *Marine Geophysical Research*, 34(3), 341–365. doi: 10.1007/s11001-013-9171-y
- [81] Flower, M., Tamaki, K., and Hoang, N., 1998. Mantle Extrusion: A Model for Dispersed Volcanism and Dupal-Like Asthenosphere in East Asia and the Western Pacific. *Mantle Dynamics and Plate Interactions in East Asia*, 27, 67–88. <https://doi.org/10.1029/GD027p0067>